2007

Liquid Crystal Thermography Studies In Water Pool Boiling At Subatmospheric Pressures

Kiran Talari

University of Central Florida

LIQUID CRYSTAL THERMOGRAPHY STUDIES IN WATER POOL BOILING AT SUBATMOSPHERIC PRESSURES

by

KIRAN TALARI
B.Tech. Indian Institute of Technology, Madras, 2004

A thesis submitted in partial fulfillment of the requirements
for the degree of Master of Science
in the Department of Mechanical, Materials and Aerospace Engineering
in the College of Engineering and Computer Science
at the University of Central Florida
Orlando, Florida

Spring Term
2007

ABSTRACT

A pool boiling experimental facility has been designed and built to investigate nucleate pool boiling in water under sub atmospheric pressure. Liquid crystal thermography, a non intrusive technique, is used for the determination of surface temperature distributions. This technique uses encapsulated liquid crystals that reflect definite colors at specific temperatures and viewing angle.

Design of the test section is important in this experimental study. Since a new TLC is required for every new set of test conditions, a permanently sealed test section is not an option. The real challenge is to design a leak proof test section which is flexible so that it can be taken apart easily. A plexiglass test section, including a top chamber with an internal volume of 60.9 x 60.9 x 66.4 mm and a bottom plate of 5.5mm thickness is designed and assembled together using quick grips. In the test section, water is boiled using 85.0mm x 16.0mm and 0.050mm thick Fecralloy® as the heating element. The TLC sheet is attached to the bottom plate and the heating element is placed on top of TLC so that the temperature distribution of the heating element during boiling can be interpreted from TLC.

A camera system fast enough to capture the thermal response of the TLC and an arrangement to capture both hue of the TLC and growth of the bubble on the same frame has been designed and successfully used. This system allowed recording of position, size and shape of the bubble with synchronized surface temperature.

In order to get hue *vs*. temperature relation, *in-situ* calibration of the TLC is performed for each test condition with the present experimental setup and lighting conditions. It is found that the calibration curve of the TLC at atmospheric pressure is different from the calibration curve of the same TLC at subatmospheric pressures. The maximum temperature difference between the two curves for the same hue is found to be only 0.6°C.

The experiment is run at four different test conditions of subatmospheric pressure and low heat flux. It is run at system pressures of 6.2kPa (0.89Psi) and 8.0kPa (1.16Psi) with a constant heat flux of 1.88kW/m^2 and 2.70kW/m^2, and a constant heat flux of 2.70kW/m^2, 3.662kW/m^2 and 4.50 kW/m^2 respectively. Analysis of nucleating surface temperatures using thermochromic liquid crystal technique is performed for these test conditions and the bubble dynamics is studied. The temperature distribution is quite varied in each case and the temperature is at its maximum value at the center of the bubble and it decreases radially from the center. The dry spot observed during the experiments indicates that the process of evaporation of the microlayer is dominant at subatmospheric pressures. It is observed that at very low pressure and heat flux the bubble growth is accompanied by the neck formation.

Boiling parameters such as bubble frequency, bubble size and contact are also analyzed and a summary of these results for four different test conditions is presented and the relevant differences between the cases are discussed and the effect of increase in pressure and heat flux is noted.

ACKNOWLEDGMENTS

I would like to take this opportunity to express my gratitude to my advisor Dr. Ranganathan Kumar for all the support and guidance he gave through out my course of graduate study. I would like to thank Dr. Jayanta Kapat and Dr. Ruey-Hung Chen for serving on my thesis committee and for their valuable suggestions. I would also like to thank my friends and colleagues.

TABLE OF CONTENTS

LIST OF FIGURES

LIST OF TABLES

LIST OF ACRONYMS/ABBREVIATIONS

CCD	Charge-Coupled Device
CHF	Critical Heat Flux
D_c	Contact diameter
D_h	Hydraulic diameter
FS	Full Scale
HSI	Hue-Saturation-Intensity
P_{sat}	Saturation Pressure
P_∞	Ambient Pressure
q”	Heat Flux
RGB	Red-Green-Blue
SEE	Standard Estimate of Error
TLCs	Thermochromic Liquid Crystals
T_s	Surface Temperature
T_{sat}	Saturation Temperature
T_w	Wall Temperature

CHAPTER 1 INTRODUCTION

1.1 Boiling Heat Transfer

Boiling heat transfer is a mode of heat transfer that occurs with a change in phase from liquid to vapor. It is an extremely important process, particularly as a method of providing high rates of heat transfer. Its sensitivity to the surface micro-geometry, wettability and to the bulk thermal properties and thickness of the heated wall, combined with the large number of potentially significant thermal and transport properties of the liquid and vapor phases, make the prediction of boiling heat transfer much more difficult and less accurate than the prediction of single-phase convection and is considered as a complex process. However, the high efficiency of boiling processes makes it the mode of heat transfer of choice for many applications including space applications. It is employed in many industrial processes because of its effectiveness in cooling. Potential applications cover not only thermal management and cooling of electronic devices, but also fluid handling and control, orbit storage and supply systems for cryogenic propellants and life support fluids, and future power systems.

1.2 Pool Boiling

Pool boiling is the type of boiling that occurs when a heater is submerged in a pool of initially stagnant liquid. When the surface temperature, T_s, of the heater sufficiently exceeds the saturation temperature, T_{sat}, corresponding to the liquid pressure, vapor bubbles nucleate on the

heater surface. The bubbles grow rapidly in the superheated liquid layer next to the surface until they depart and move out into the bulk liquid.

While rising as the result of buoyancy, they either collapse or continue their growth, depending upon whether the liquid is locally subcooled or superheated.The pool boiling process is made up of four regimes that include natural convection, nucleate boiling, transition boiling and film boiling .The behavior of the boiling curve in each of these four regimes is shown in Figure 1.1.

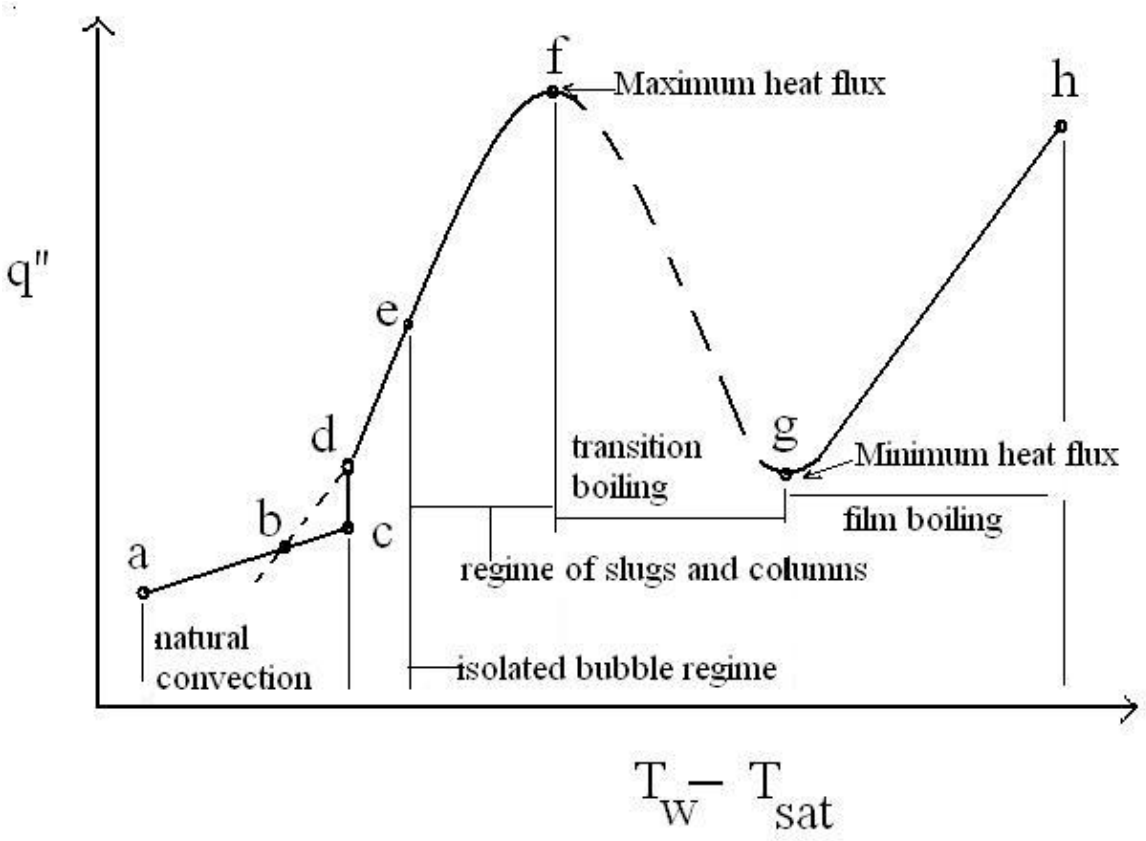

Figure 1.1: Pool boiling regimes for an independently controlled surface temperature

1.2.1 Natural Convection

Natural convection exists at low superheats. At low superheats, nucleation sites may not be active and heat is transferred to the ambient liquid from the wall surface by natural convection as shown in Figure 1.2. The nucleation sites are deactivated by penetration of the colder bulk liquid into cavities of the material, which prohibits bubbles from growing and releasing. Some vapor may exist, but the interior vapor pressure is not high enough (relative to the vapor pressure) to allow the bubble embryo to grow and nucleate.

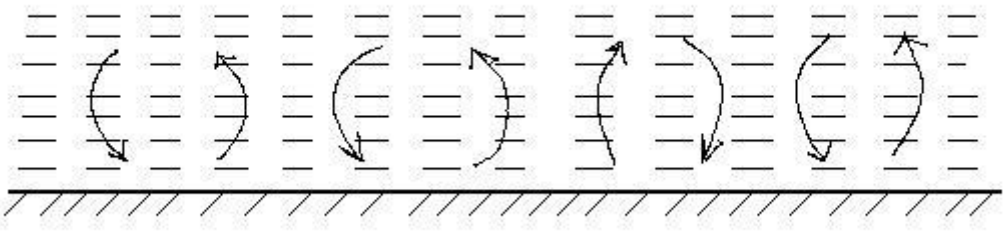

Figure 1.2: Natural Convection

At the boiling point, bubbles start to form when more heat is generated at the surface. This allows the nucleation sites to become active as shown in Figure 1.3.

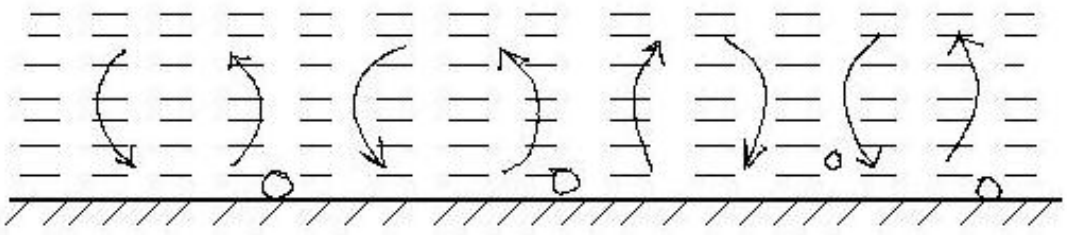

Figure 1.3 Onset of boiling

1.2.2 Nucleate Boiling

Nucleate boiling occurs when bubbles begin to form on the heated surface. In the first regime of nucleate boiling, isolated bubbles form at nucleation sites, which depart from the heated surface as seen in Figure 1.4. This allows the ambient fluid to mix near the surface, increasing the heat transfer coefficient. Most heat transfer in this regime is from direct transfer between the solid and liquid via the motion of the liquid. Vapor within the bubbles does not play a major role in the actual heat transfer.

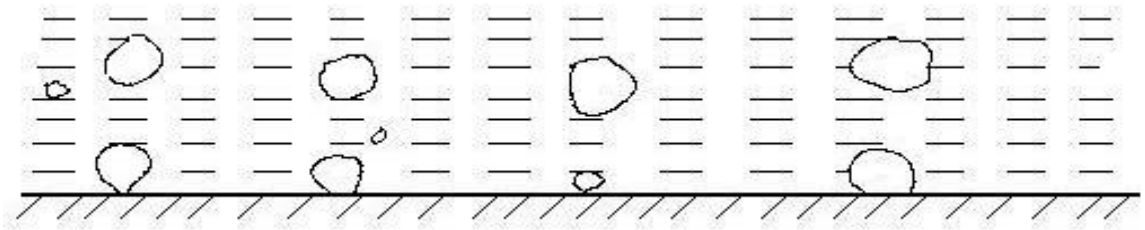

Figure 1.4: Isolated bubble regime

At higher heat fluxes, however, nucleation sites become more numerous. The active nucleation sites are close enough together so that bubbles begin to interfere with each other. In this regime, vapor is being produced so quickly that bubbles merge into columns or slugs as seen in Figure 1.5. This continues to occur as heat flux rises until the heat flux reaches the critical heat flux (CHF).

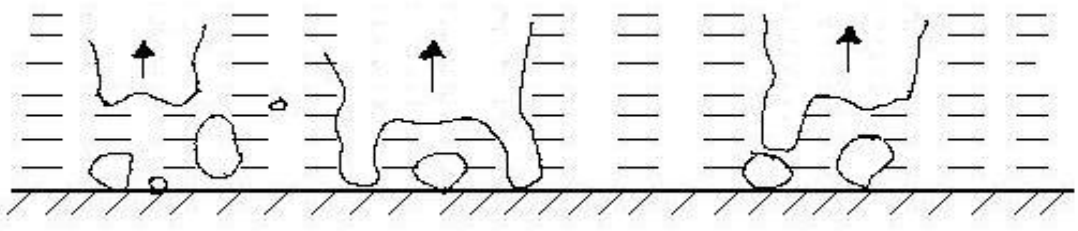

Figure 1.5 :Regime of slugs and columns

The critical heat flux (CHF) is where the boiling curve heat flux reaches a maximum while transitioning between nucleate and transition boiling.

1.2.3 Transition Boiling

A reduction in heat flux and a significant increase in superheat are observed during the transition boiling. As superheat increases, bubble formation becomes more rapid, and a film of vapor increasingly covers the heated surface as shown in Figure 1.6. Since the vapor has a lower thermal conductivity than the liquid, the heat transfer rate decreases rapidly. In this region, fluctuations between film boiling and nucleate boiling occur. As wall superheat intensifies, film boiling increases while nucleate boiling decreases.

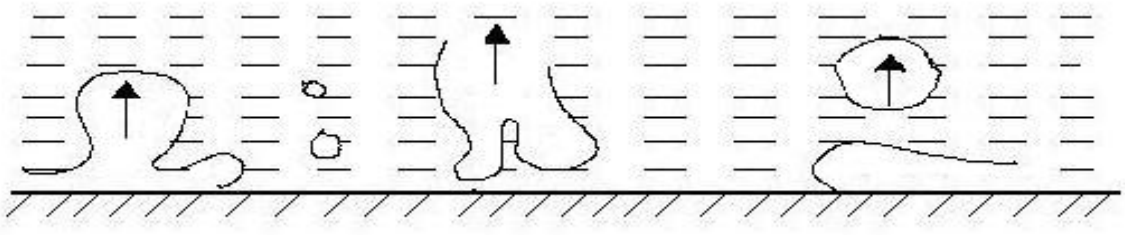

Figure 1.6: Transition boiling

In the case of constant heat flux surface, however, the transition boiling does not occur. The dip in the curve following maximum heat flux is replaced by a horizontal line leading to film boiling. Thus at CHF, for a negligible increase in heat flux, there is a sudden jump in (T_w-T_{sat}).

1.2.4 Film Boiling

Film boiling occurs at the Leidenfrost point, when heat flux reaches a minimum after CHF. At this point, a vapor blanket completely covers the heated surface as seen in Figure 1.7. Heat is transferred from the surface to the liquid only by conduction and radiation but because of an increase in surface temperature, radiation may become more significant. Superheat in this regime can be high enough to melt or destroy the surface.

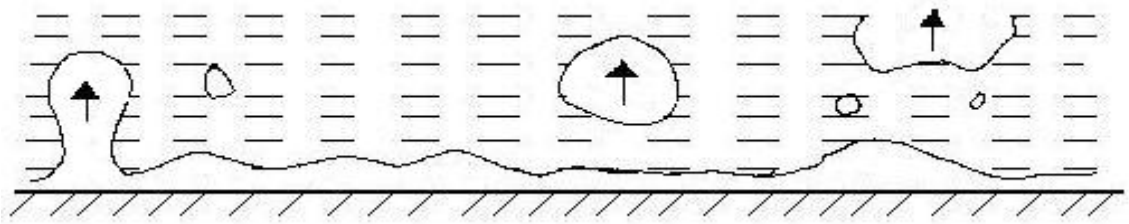

Figure 1.7: Film Boiling

1.3 Pool Boiling of water at subatmospheric pressures

In applications where it is desirable to keep the temperature of a boiling surface low, reducing the saturation pressure may be a useful solution. Higher heat fluxes from current electronic components are not easily handled by solid heat sinks. The use of phase-change heat sinks, which operate with a nearly isothermal interior, is becoming more common. Low temperature operation of these heat sinks may be prescribed by creating saturated liquid and vapor state in the

vessel at very low pressures. Therefore the boiling occurs in the heated end of the vessel at a low temperature.

A reduction in the saturation pressure causes a corresponding decrease in the saturation temperature, also called boiling temperature. This temperature decrease is translated to the boiling surface .This is particularly useful when water is used as the boiling liquid. Water is a desirable liquid since it has a high heat of vaporization, high thermal conductivity, and is non-toxic and non-flammable.

Pool boiling heat transfer of water has been investigated extensively by many researchers at system pressure varying from atmospheric to near critical pressure. However, at subatmospheric pressure conditions there is a dearth of data, particularly when the vapor pressures are very low. The characteristics of pool boiling of water at low pressure are much different from pool boiling at atmospheric pressure. Thus, this study is partly motivated in obtaining experimental data at subatmospheric pressure in pool boiling to understand boiling characteristics in such conditions.

1.4 Thermochromic Liquid Crystals (TLCs)

Nucleate boiling represents an example in which the underlying processes are strongly non-linear and not completely understood. Better understanding of the information available from spatio-temporal experiments is required to advance our current understanding of the physics of nucleate boiling, thereby allowing improved industrial applications.

In recent years, Thermochromic Liquid Crystals (TLCs) have been successfully used in non-intrusive heat transfer studies. TLCs react to change in temperature by color. The TLC based temperature visualization is based on the property of some cholesteric and chiral-nematic liquid crystal materials to reflect definite colors at specific temperatures and viewing angle. The color change for the TLC ranges from clear at ambient temperature, through red as temperature increases and then to orange, yellow, green, blue and violet before turning colorless(isotropic) again at a higher temperature. They appear colorless above and below the active range. Since the color change is reversible and repeatable, they can be calibrated accurately with proper care and in this way as temperature indicators.

Thin coatings of TLCs at surfaces are utilized to obtain detailed heat transfer data of steady or transient process. Rapid developments of the hardware, software and computerized image processing techniques have made it possible to setup inexpensive system capable of real-time transient full-field temperature measurements using TLCs.

1.5 Objectives

A research program was undertaken to use Thermochromic Liquid Crystals (TLCs) for surface temperature measurements in a two-phase pool-boiling environment.

The main objectives of this research are outlined as follows:

1) To setup a leak proof pool boiling facility for water at subatmospheric pressures.

2) To calibrate the TLC at different pressures.

3) To collect the TLC image data set.

4) To develop the software to process TLC images to get the required temperature data.

5) To synchronize the corresponding bubble formation information with the wall temperature measurements.

A test section made of plexiglass was used for these experiments. The experimental loop was carefully fabricated to make sure that the loop, with all its components, including the test section withstands subatmospheric pressures.

In the bottom surface of the test section, electrical heating was achieved using 0.05mm Fecralloy® sheet with a 30μm TLC paint backed by a transparent 125μm layer of Mylar.

A 3CCD RGB camera was setup below the test section for observation of hue on TLC coated surface, while a mirror arrangement was used to get the bubble growth information. *In-situ* calibration was performed to get hue *vs.* temperature relation. The TLC images were collected during the boiling process and analyzed to get the detailed wall temperatures. The wall temperatures were plotted for selected regions on the heated surface at and near the nucleation site(s).The synchronized bubble formation information, in combination with the wall temperatures was used to study the bubble dynamics.

CHAPTER 2 LIQUID CRYSTAL THERMOGRAPHY

2.1 Thermo (temperature) Chromic (color) Liquid Crystals

Liquid Crystals that show different colors at different temperatures because of the selective reflection of specific wavelengths of light from their structures are called thermochromic liquid crystals.

Cholesteryl esters have been known as thermochromic liquid crystals since the 1960s. The cholesteryl nonanoate, an example of cholesteryl esters is shown in Figure 2.1.

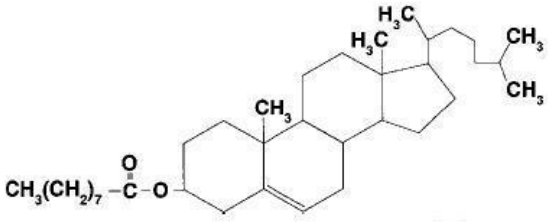

Figure 2.1: Thermochromic liquid crystal: cholesteryl nonanoate [1]

The instability of cholesteryl esters to oxygen and ultraviolet light has severely restricted their use. The search for improved liquid crystal display materials led to the discovery of thermochromism in cyanobiphenyls, shown in Figure 2.2.

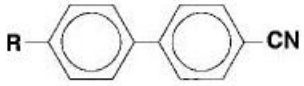

Figure 2.2: Thermochromic liquid crystal: cyanobiphenyl [1]

2.1.1 History of Liquid Crystals

Liquid crystals are chemical compounds and mixtures that exhibit the mechanical properties of liquids and the optical characteristics of solids. These were discovered in 1888 by Austrian botanist Friedrich Reinitzer when he was studying the melting behaviour of cholesteryl benzoate. He noticed the appearance of a turbid fluid at 145.5°C which did not form a conventional clear liquid until 178.5°C. He concluded that a new state of matter had been discovered that was intermediate in ordering between the crystalline solid and isotropic liquid phases. Accordingly, this intermediate phase became known as the liquid crystal phase or mesophase.

Much research in the early days provided information on the nature of the liquid crystal phase and many different types were discovered. However, the significance of liquid crystals in technological devices (e.g., displays and thermography) was not realized until the 1960s. More importantly, it was not until the discovery of stable, room temperature, nematic liquid crystals by George Gray (an organic chemist) at the University of Hull in 1973 that liquid crystal displays could be made commercially viable.

Many different liquid crystalline materials are now known and they generate a wide range of different liquid crystalline phase types. The intense research into the design, synthesis, evaluation and applications of liquid crystal materials has provided a wide range of quality liquid crystal displays and a multitude of thermochromic devices.

2.1.2 Liquid crystalline mesophase

A material is defined as a crystalline solid (Cryst) when the structure has long-range order of the molecular positions in three dimensions. A fully ordered crystal will also have long-range orientational ordering of its constituent molecules.

When a fully ordered molecular crystal is heated the thermal motions of the molecules within the lattice increase and eventually the vibrations become so intense that the regular arrangement of molecules is broken down with the loss of long-range orientational and positional order to give the disorganised isotropic liquid (Iso). The temperature at which this process occurs is called the melting point and the heat absorbed by the molecules is the latent heat of fusion. However, this process, which takes a compound from being very well ordered to being totally disordered in one step, is a very destructive one, which is not universal for all compounds. For many compounds, this process occurs by way of one or more intermediate phases as the temperature is increased.

These phases are called mesophases and some of these mesophases are liquid crystalline.Liquid crystalline phases have properties which are intermediate between those of the fully ordered crystalline solid and the isotropic liquid. Liquid crystalline mesophases are fluids which, due to partial orientational ordering of the constituent molecules, have material properties such as permittivity, refractive index, elasticity and viscosity which are anisotropic (*i.e.*, their magnitude will differ from one direction to another).

The liquid crystals are made up of long-chain organic molecules that can exist in either the smectic or nematic phase. In the smectic phase, all the molecules are layered with long axes oriented (or nearly oriented) in one particular direction. In the nematic phase, the molecules are not layered, but the long axes of nearby molecules are still oriented nearly in one particular direction.

The cholestric liquid crystals are the molecules which are in the nematic phase and also chiral, i.e., the molecules are not symmetric about their long axis. These molecules are oriented in a preferred direction but the direction of preferred orientation varies periodically on passing through the material, as shown in Figure 2.3.

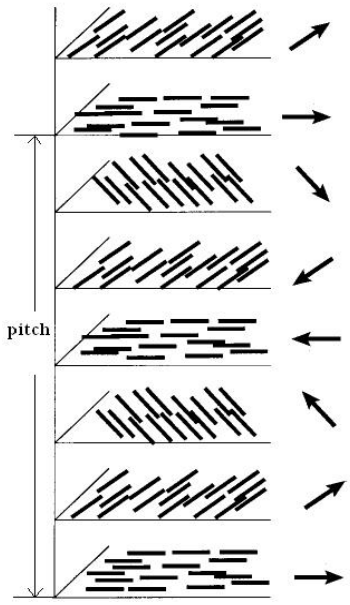

Figure 2.3: The orientation of molecules in cholestric liquid crystal [1]

The pitch is defined as the repeat distance along the direction of periodicity; that is, different layers separated by the pitch (or an integer multiple of the pitch) have the same orientation.

Typical values of the pitch can be of the order of the wavelength of visible light (400 to 700nm). As a result, visible light can undergo Bragg reflection from the subsequent layers, and the color of the liquid crystal will correspond to the wavelength of light for which maximum interference occurs. An illustration of the effect of thermochromism in a cholesteric liquid crystal is shown in Figure 2.4.

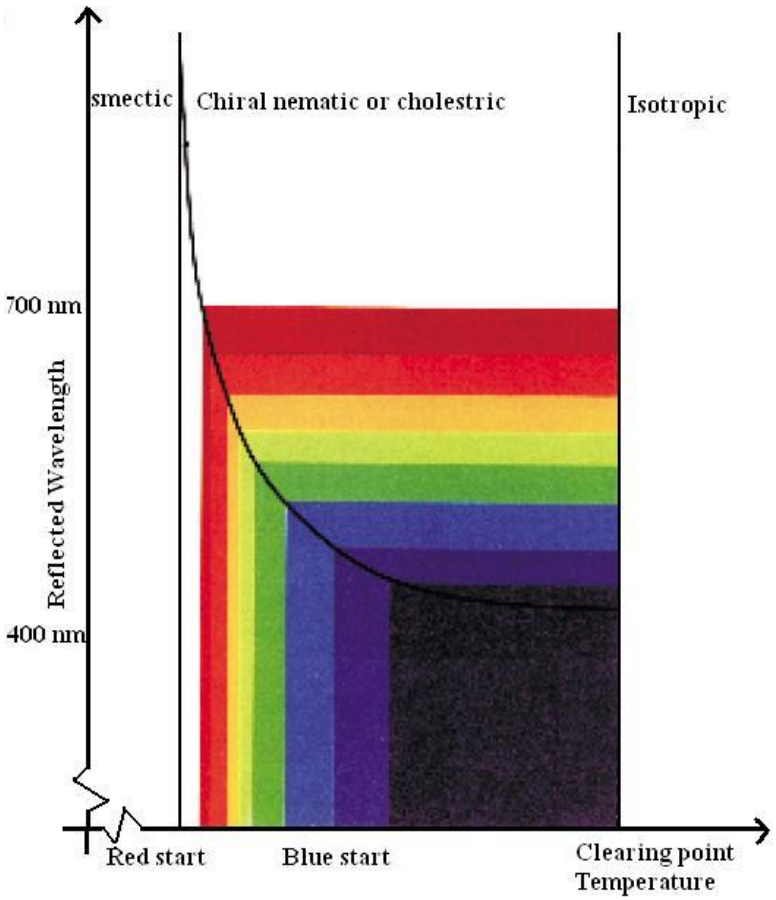

Figure 2.4: The relation between temperature and wavelength [2]

In a cholesteric liquid crystal, changes in temperature result in thermal expansion, which leads to a change in layer spacing and hence pitch, and therefore the color observed will vary with temperature. Since the pitch varies continuously as the temperature changes, the color will change from black to red through orange, yellow, green, blue, violet, and again black.

Thermochromic liquid crystals can have a versatile range of colors and useful color changes from -30°C to above 120°C, often with very high temperature sensitivity.

2.1.3 Micro-encapsulation

The TLCs come in two packaged forms, raw mixtures and micro-encapsulated particles. In simple terms, a microcapsule is a small sphere with a uniform wall around it, and in the micro-encapsulation process tiny droplets of liquid crystal are surrounded with a continuous polymer coating to give discrete microcapsules. Microcapsule diameters are generally between a few microns and a few millimeters.

The advantage of micro-encapsulation is that the TLCs are protected from external contamination. Thus micro-encapsulated TLC particles have a much longer life than unprotected raw TLC particles that are made by dicing raw TLC mixtures.

2.1.4 Time response and accuracy of TLCs

The response time of TLCs vary from 2ms to above 10ms, depending on the application. It has been observed in earlier experiments that through proper calibration, color can be correlated with temperature to within approximately ± 0.1 to 0.3°C.

2.2 Measurement System of TLC

The essential elements of measurement system of TLC used in the experiments include illumination source, 3 CCD RGB camera and data acquisition/processing units.

2.2.1 Illumination Source

A bright and stable white light source was used to obtain accurate and reliable reflected light intensity from a TLC coated surface. Any IR energy present in the incident light will cause the radiant heating of the test surface and extended exposure to UV radiation can cause rapid deterioration of the TLC surface. Hence light source was chosen to be void of infrared (IR) and ultra-violet (UV) radiation.

2.2.2 CCD camera system

The CCD (Charge-coupled Device) camera system used for image acquisition was a JAI MV90 3 CCD color camera .The camera was interfaced with the CPU using a frame grabber embedded, which converted the analog signals from the camera into digital RGB images. The frame grabber was a Coreco PC-RGB 24 bit color frame grabber.

A CCD type camera (Analog and Digital) image sensor uses photo diodes to convert photons to electrons. CCD sensors create high quality, low-noise images. An image sensor consists of a

rectangular array (imagers) or a single line (line-scan) of equi-spaced, discrete light-sensing elements, called photo-sites.

The charges that build up on all of the array photo-sites were linked or "coupled" together so that they could be transferred out of the array directly (digital output) or processed into a time-varying video signal (analog output) . A visual representation of an image sensor is shown in Figure 2.5.

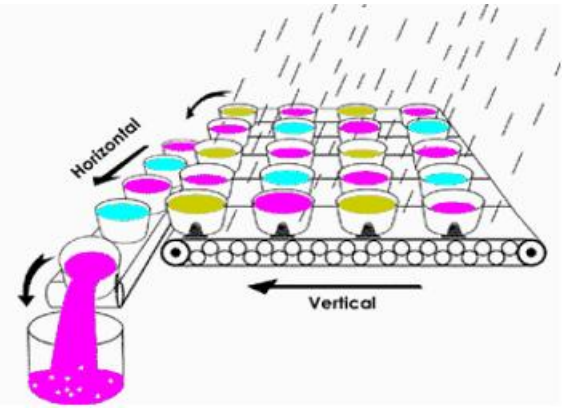

Figure 2.5: Visual Representation of an image sensor

As shown in the figure above, the image sensor could be represented in the form of an array of buckets (photo diodes). Whenever the buckets were filled with sufficient amount of light (pixels), they were transferred.

The camera in this experiment was an analog camera. The final output from an analog camera would be an analog signal, which needs to be processed further so that a digital image can be captured. This was accomplished using the Coreco PC-RGB 24 bit color frame grabber.

2.3 The Hue Technique

Liquid crystal imaging is ideal for producing a qualitative picture of two-dimensional field in which the temperature varies both spatially and temporally. Quantitative measurements, however, are more difficult. In practice, a quantitative measurement system requires that temperature be associated with a measurable scalar that represents the `color' of the liquid crystal surface at every pixel in an image field.

The image of a TLC surface captured is a red-green-blue (RGB) image, where the color of each pixel is described by red, green, and blue intensity values. The three independent coordinates of the RGB color model can be mathematically transformed into any other set. The most useful of these is the hue−saturation−intensity (HSI) color model, where intensity is a measure of the brightness, saturation is a measure of the depth of the color, and hue is a measure of the dominant wavelength. The hue of the color can be represented as the angle resulting from a vector rotating about the white point (R=G=B point), as shown in Figure 2.6.

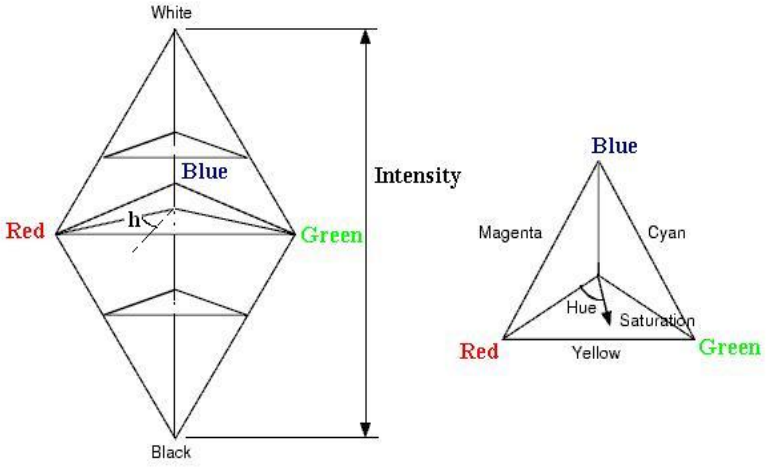

Figure 2.6: HSI triangle model

As TLCs reflect light at a wavelength dependent on temperature, the hue of the reflected light is also a function of temperature. Therefore, if the RGB image of a TLC surface is converted to an HSI image, the hue value of each pixel indicates the temperature of the corresponding location on the surface. Such color spaces are not unique, and a number of different definitions of hue, h, can be found in the literature.

In earlier studies, researchers evaluated three common color spaces and found that their definition for hue, h, as given by Equation. 2.1, yields the lowest average uncertainty while retaining computational simplicity.

$$h \equiv \arctan\left(\frac{\sqrt{3}(G-B)}{2R-G-B}\right) \tag{2.1}$$

The color response is calibrated against temperature by building an analytical relation between the temperature and the hue of the color. A suitable polynomial fit is then used to describe this

relation. These polynomial coefficients are used in calculating the temperature values from the TLC image.

2.4 Limitations of Liquid Crystal Thermography

In nucleate boiling, the heat fluxes and fluid-side heat transfer coefficients are high. There is no clear view of the surface from the fluid side and the heat transfer processes are sensitive to the state of the surface and the thermal properties of the wall. This means that the liquid crystal can only be applied to the rear surface of a thin metal plate that is heated internally by ohmic resistance heating.

The requirement for a thin wall reduces the thermal capacity of the plate and restricts lateral conduction, thus altering the boiling processes that are under investigation. Thermochromic liquid crystals are only useful when they are in the liquid crystalline phase, which is a mesophase (an intermediate phase of matter) between an isotropic liquid (high temperature) and crystalline solid (low temperature), which restricts the temperature range of their applicability.

The calibration of hue component against temperature is sensitive to the nature and angle of illumination and the angle of viewing .Therefore the calibration should be performed *in- situ*. The calibration also depends on every component in the image processing chain. However, TLCs have many advantages including, easy handling, low cost, nearly instant measurement and good accuracy, and resolution.

CHAPTER 3 BACKGROUND AND LITERATURE REVIEW

3.1 Introduction

The phenomenon of two-phase boiling heat transfer is considerably more complicated than single-phase heat transfer. This is because not only the variables associated with single-phase heat transfer are involved, but also those variables associated with the phase change must likewise be considered. As a result of the large number of variables, neither general equations describing all the boiling processes or general correlations of the boiling heat transfer have been developed.

The importance of boiling in thermal systems has been an incentive for the heat transfer community to study the nature of this phenomenon for more than half a century. Extensive data have accumulated from experimental studies carried out under various conditions and configurations, leading to the development of currently available empirical correlations. But, the development of mechanistic models based on the underlying physical processes has been limited.

The primary goal of the recent studies has been to construct boiling models based on the physical sub-processes associated with the bubbling events. Although the developed models are intended to predict the heat transfer coefficient at macroscales, their fundamental assumptions are founded on complex microscale sub-processes that remain experimentally unverified.

3.2 Bubble Growth Mechanism

3.2.1 Homogeneous Nucleation Process

Bubble nucleation completely within a superheated liquid is called homogeneous nucleation. Many of the more complex features of bubble growth near a heated solid surface are absent for these circumstances.

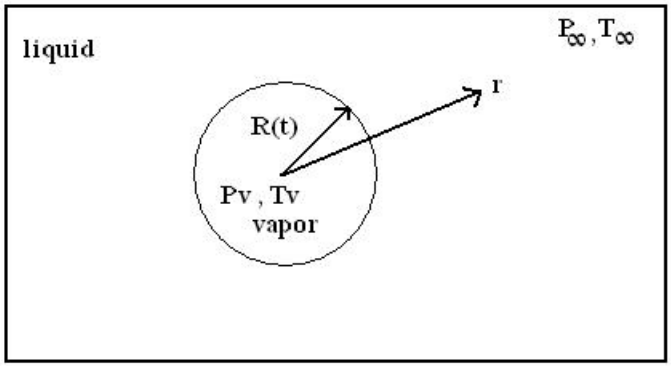

Figure 3.1: Bubble growing in superheated liquid

For the bubble shown in Figure 3.1, at any instant during the growth process, the interface is located at r = R and is moving with a velocity dR/dt relative to the reference frame. The pressure and temperature are P_v and T_v inside the bubble and P_∞ and T_∞ in the surrounding liquid, respectively.

When the bubble first forms, the interface temperature will be nearly equal to the superheated liquid temperature, and the vapor generated at the interface will be at a pressure nearly equal to P_{sat} (T_∞). As the liquid superheat near the interface is consumed to provide the latent heat of

vaporization, the temperature at the interface will drop toward T_{sat} (P_∞). During the bubble growth process, the capillary pressure difference across the interface decreases as the radius increases, and the pressure inside the bubble drops toward P_∞. During the growth process, P_v and T_v will therefore lie in the ranges

$$P_\infty \leq P_v \leq Psat\ (T_\infty) \tag{3-2}$$

$$T_{sat}\ (P_\infty) \leq T_v \leq T_\infty \tag{3-3}$$

Inertia-controlled growth and Heat-transfer-controlled growth are the two limiting cases of the bubble growth process.

3.2.1.1 Inertia-controlled growth

During inertia-controlled growth, P_v is near its maximum value. P_{sat} (T_∞), and $T_v \cong T_\infty$. Heat transfer to the interface is very fast and is not a limiting factor to growth. The growth rate is therefore governed by the momentum interaction between the bubble and the surrounding liquid. These conditions usually exist during the initial stages of bubble growth, just after the embryo bubble forms and begins to grow.

3.2.1.2 Heat-transfer-controlled growth

During heat-transfer-controlled growth, T_v is near its minimum value, T_{sat} (P_∞) and $P_v \cong P_\infty$. Growth is limited by the relatively slower transport of heat to the interface. As a result, the interface motion is slow compared to that for inertia-controlled growth, and the momentum

transfer between the bubble and the surrounding liquid is not a limiting factor. These conditions generally correspond to the later stages of bubble growth when the bubble is larger and the liquid superheat near the interface has been significantly depleted.

The growth of a bubble in a superheated liquid was studied by Bosnjakovic [3] and Fritz and Ende [4]. They assumed that the heat required for liquid evaporation at the bubble/liquid interface is supplied by conduction through a thermal boundary layer surrounding the bubble. They suggested that since the thermal boundary layer thickness is small compared to the bubble radius, heat transfer to the interface can be approximated using the solution of transient heat conduction in a semi-infinite solid.

Foster and Zuber [5] and plesset and Zwick [6] presented the first analysis of the bubble growth in a superheated liquid that incorporated both momentum and energy transfer effects.

3.2.2 Heterogeneous Nucleation Process

The growth of vapor bubbles in the thermal boundary-layer region near a superheated surface is more complex. The existence of the heating surface in heterogeneous bubble growth leads to:

- The lack of spherical symmetry
- The presence of non-uniform temperature field in the surrounding liquid

The lack of understanding of the physics of these contributing factors has made it very difficult to predict the bubble growth in the heterogeneous boiling process. Hence this boiling process can

be considered as one of the most complicated process. Despite these significant differences, bubble growth near a superheated surface exhibits regimes of inertia-controlled and heat-transfer controlled growth similar to those for spherical bubble growth in an infinite, uniformly superheated ambient.

During the bubble growth process near a heated wall, after the departure of a bubble, liquid at the bulk fluid temperature T_∞ is brought into contact with the surface at temperature $T_w > T_{sat}$ (P_∞). A brief period of time then elapses, during which transient conduction into the liquid occurs but no bubble growth takes place. This time interval is referred to as the waiting period, t_w.

Once bubble growth begins, the thermal energy needed to vaporize liquid at the interface comes, at least in part, from the liquid region adjacent to the bubble that was superheated during the waiting period. As the bubble embryo bubble emerges from the nucleation site cavity, a rapid expansion is triggered as a result of the sudden increase in the radius of curvature of the bubble. As the bubble grows radially, a thin microlayer of liquid is left between the lower portion of the bubble interface and the heated wall. This film, which is called the evaporation microlayer, varies in thickness from nearly zero near the nucleation site cavity to a finite value at the edge of the hemispherical bubble. Heat is transferred across this film from the wall to the interface. This film may completely evaporate near the cavity where nucleation begins, significantly elevating the surface temperature there. When this occurs, the surface temperature may strongly fluctuate during the repeated growth and release of bubbles as the surface cyclically dries out and then rewets.

3.2.2.1 Bubble growth due to heat transfer from relaxation microlayer

The liquid region adjacent to the interface is gradually depleted of its superheat as the bubble grows. This region is called the relaxation microlayer.

Numerous studies have been conducted in the past to understand the physics of the heterogeneous bubble growth. Johnson et al. [7] provided images of bubbles generated under a wide range of conditions on a heated wall. They noted that all the bubbles finally approach a spherical shape before departure, regardless of their initial shape.

Bubble growth in a non-uniform temperature field was considered by Griffith [8], Savic [9] and Bankoff and Mikesell [10]. Their solutions for bubble growth have often led to complex expressions that are impractical to use. Cole [11] accounted for non-uniformity of the temperature by using half of the wall actual superheat in the formula for bubble growth in a uniformly superheated liquid.

The model of Mikic and Rohsenow [12] treats the heat-transfer-controlled growth as being governed by a one-dimensional transient conduction process that consists of two parts. Based on this model, heating of the liquid starts at $t = - t_w$, which is the beginning of the waiting period. During this waiting process, transient conduction in the liquid is postulated to satisfy the one-dimensional transport equation with appropriate boundary and initial conditions.

At the second stage of the process, when a bubble forms on the surface ($t > 0$), heat transfers from the semi-infinite body of liquid to the bubble/liquid interface that is taken to be at $T_{sat}(P_\infty)$.

The R(t), radius growth, relation for heat-transfer-controlled growth obtained by Mikic and Rohsenow is not accurate when inertia effects are significant and hemispherical growth occurs. For such conditions, vapor production at the interface of the evaporation microlayer at the base of the bubble plays a major role and must be incorporated into the bubble growth model. Analytical models of the transport in the evaporation microlayer have been proposed by Cooper and Lloyd [13] and Van Stralen et al. [14] suggested that the superheated liquid adjacent to the surface is normally thin and does not necessarily cover the entire bubble.

3.2.2.2 Bubble growth due to heat transfer from evaporation microlayer

Through direct measurement of surface temperature, Hsu and Schimdt [15], Moore and Mesler[16], Rogers and Mesler[17] and others discovered that the surface temperature beneath a bubble significantly drops on the onset of nucleation. These observations led to a new theory for bubble growth that reshaped the discussion about the bubble growth mechanism over the following years.

It is postulated that the quick cooling process is caused by evaporation of a thin layer of liquid that gets trapped beneath the bubble during the initial phases of the bubble growth.The first actual verification of the microlayer existence was conducted by Sharp [18] using interferometric techniques coupled with high speed photography.

Cooper and Lloyd [13] conducted an experimental/analytical study, in which they measured the surface temperature of a heated glass substrate beneath a bubble generated in boiling of toluene at subatmospheric pressures (7-14 kPa). The generated bubbles were hemispherical during the growth process and grew to a diameter of about 20mm before departure. Cooper and Lloyd [13] calculated the heat flux at the bubble/surface interface using the surface temperature data. The calculated heat flux was used to determine the microlayer thickness.

Their measurements indicated a wedge-shaped microlayer, increasing from the bubble center to the bubble edge with a maximum thickness of about 30-50 μm. Comparison of the calculated heat flux values with the total energy transferred into the bubble (determined using the bubble volume) suggested that microlayer played a predominant role in the bubble growth. In describing the physics of the microlayer formation, they argued that a growing bubble overtakes some of the boundary layer liquid and a balance between the inertia, viscosity and surface tension forces determine the thickness of the trapped liquid layer. They argued that factors tending to make bubbles grow rapidly to large size would tend to encourage formation of a microlayer and also make the bubble of hemispherical shape, with a large area of contact at the wall, hence giving a large area for microlayer development.

3.3 Bubble departure diameter and the frequency of bubble release

The complete process of liquid heating, nucleation, bubble growth, and release, collectively referred to as the ebullition cycle, is the central mechanism of heat transfer from a superheated wall during nucleate boiling. Two features of this process that affect the rate of heat transfer

during the ebullition cycle are the bubble diameter at departure, D_d, and the frequency, f, at which bubbles are generated and released.

The departure diameter of bubbles during nucleate boiling has been the subject of numerous investigations over the past few decades. In experimental studies, the departure diameter was typically determined from high-speed movies of the boiling process. Based on data obtained in this manner, a number of investigators have proposed correlation equations that can be used to predict the departure diameter of bubbles during nucleate boiling.

3.4 Nucleate boiling studies at subatmospheric pressures

The characteristics of pool boiling of water at low pressure are much different from pool boiling at subatmheric pressures. Cryder and Finalborgo discussed the gross effects of low pressure on heat transfer. Raben et al. [19] investigated saturated nucleate pool boiling of water at subatmheric pressures from a 38.1 mm diameter horizontal heated surface. The objective of their investigation was to identify the dominant energy transport mechanisms of nucleate boiling and understand how they are affected by pressure. By applying the energy equation to a simple heat transfer model, they presented a theoretical analysis of nucleate boiling.

They postulated that free convection, vapor-liquid exchange, and the latent heat of vaporization are the modes in which energy is transferred during saturated nucleate boiling. For very low pressures they found that the contribution of latent heat was insignificant compared to the vapor-liquid exchange.

The departure of vapor bubbles in water at low pressure has been the subject of several other studies, which have uncovered several important features of this boiling process. Cole and Shulman [20] measured and correlated the effect of pressure on bubble departure diameters from a thin 12.7 x 101.6 mm horizontal zirconium ribbon.

Van Stralen et al. [21] have studied nucleate boiling in an extensive liquid pool of water at subatmheric pressures. They have investigated the growth rate of vapor bubbles experimentally up to departure in water boiling at pressures varying from 26.7 to 2.0 kPa. Comparison of their data with existing theory showed the substantial influence of liquid inertia during initial growth.

They have observed a curious bubble cycle at very low pressures in the order of 2kPa.They have noticed that directly after departure of a large bubble, an initially very rapidly growing thin vapor column occurred at the nucleation site. This secondary bubble penetrated into the flattened lower boundary of the preceding large bubble. They attributed the curious behavior of the secondary vapor column to the occurrence of a dry area beneath the center of the growing primary bubble during adherence to the wall.

Niro and Beretta [22] examined the boiling regimes of water and acetone at low pressure in a closed two-phase thermosyphon. In their experiments they measured the bubble departure frequencies as a function of pressure and power. The heated section of their experiment consisted of 200mm long pipes of 12 and 30 mm I.D.

McGillis et al. [23] investigated boiling water at low pressures from a small horizontal thermosiphon surface. Particularly, the surface temperature oscillations caused by departing, large bubbles are described.

Ng Kim Choon et al. [24] have conducted a detailed study of pool boiling of water in an evaporator where its system pressure was about 1.8kPa.They proved that the existing boiling correlations are not applicable for system pressures that are subatmospheric.

McGillis and Carey [25] examined saturated pool boiling of water at low pressures from a heated, 12.7 x 12.7 mm horizontal surface. They explored pool boiling enhancement techniques on a horizontal surface in a thermosiphon. They proved that the size and geometry of surface enhancements effect the bubble formation, release mechanisms, and convective transport. They stated that surface enhancements often decrease the wall superheat significantly.

J.Pakleza et al. [26] performed an experimental investigation of a vapor bubble growth for water boiling inside a $30cm^3$ cube shaped cavity. Isolated bubbles were generated on a horizontal surface for their study. They measured temperature in the liquid in the upper part of the cavity and 1mm below the boiling surface using K-type thermocouples with an accuracy of ±0.5°C. In these experiments, the bulk temperature of the liquid varied in the range 25°C – 40°C. The temperature of the heated surface T_w was in the range 43°C -72°C. Their objective was to provide data in order to validate numerical models. In their study, they have noticed that due to the experimental conditions, strong vaporization dominates everywhere on the interface at early stages then condensation occurs at the bubble base that shrinks until the bubble lifts-off. Their

investigation showed that the closing down process, leading to bubble departure, induces high velocities at the bubble base.

Modelling requires experimental input about localized events. High-speed liquid crystal thermography is capable of providing detailed examples of local mechanisms of heat transfer that should be considered for incorporation in models of nucleate boiling. The color image processing is used to obtain quantitative temperature information from a TLC coated surface with a reasonable accuracy and resolution.

3.5 Nucleate boiling studies using Liquid crystal thermography

Cholesteric liquid crystals have been employed in a number of interesting applications over the past several years. The majority of uses have involved qualitative interpretation and quantitative representation of the temperature fields displayed colorfully by the liquid crystals, that is to say, observing hot and cold regions without regard to precise temperature levels. Liquid crystals have been used to observe regions of overheating on electronic equipment to check for flow blockages in heat exchangers.

Several investigators have employed liquid crystals as the temperature transducer in engineering heat transfer studies. Raad and Myers [27] pioneered the technique of using liquid crystals to observe nucleation sites in a study of pool boiling. Their liquid crystal had a color play range of only 2°C.

Kenning [28] used thermochromic liquid crystals with a color play over the temperature span 104-132°C to investigate wall temperature patterns in nucleate boiling. He measured temperature patterns on the back of a 0.13mm thick stainless steel heated plate during pool nucleate boiling of water at atmospheric pressure. He presented experimental evidence for large spatial variations in wall superheat in nucleate boiling on thin walled tubes and plates and on thick plates made of materials of moderate thermal conductivity like stainless steel.

Bergez [29] reported time-dependent study on nucleate boiling on thin plate in well-wetted conditions for water at a saturation, atmospheric pressure, and low heat flux by using simultaneous recordings of ebullition and wall temperature measurement using liquid crystal thermography. He indicated that existing heat transfer descriptions are not adequate in this case. Based on the wall temperature variations he gave a non-predictive model of boiling heat transfer with two superheats, combining heat supply and activity of nucleation site.

Kenning, Kono and Wienecke [30] investigated pool boiling heat transfer in water at 101kPa by liquid crystal thermography. Their study revealed the importance of liquid crystal thermography in providing detailed examples of local mechanisms of heat transfer that should be considered for incorporation in models of nucleate boiling.

Kenning and Yan [31] studied features of pool boiling heat transfer on a thin plate using liquid crystal thermography. They used 28.1 x 40.8mm and 0.13 mm thick stainless steel plate as a heater to boil water at atmospheric pressure. They recorded color play of the TLC and the bubble activity simultaneously using a NAC 200 color video camera. Their

measurements confirmed the importance of variations in wall temperature for the removal of heat by bubbles and the activity of nucleation sites. Their results were also consistent with evaporation of a liquid microlayer.

CHAPTER 4 EXPERIMENTAL SETUP AND PROCEDURE

4.1 Introduction

An experimental facility was set up to examine the saturated pool boiling of water at low pressures from a 85.0mm x 16.0mm and 0.05mm thick horizontal Fecralloy® surface. In order to run experiments at subatmospheric pressures it was required to design a test section that could best handle the working fluid and operating pressure and temperature. It was necessary to take apart the test section and replace the TLC for every new set of test conditions. This led to a very flexible design of the test section. A camera system that was fast enough to capture the nucleation and departure of a single bubble in multiple frames was designed. This camera system was used to study the bubble dynamics and also to provide the color images of the TLCs.

4.2 Modules of the Experiment

The modules of the experiment were as follows:

- Test Section
    - Main Chamber
    - Working Fluid
    - Heating Element
    - TLC Sheet
- Vacuum pump
- DC power supply

- Measurement devices

4.2.1 Test Section

Designing of the test section was very crucial to carry out this particular experimental study. During the initial stages of the project, an attempt was made to use an aluminum test section. This was provided with a glass window on the side to study the bubble dynamics and a quartz window was mounted on the bottom to view TLC. The aluminum test section was anodized inside to avoid corrosion from the working fluid. This required more illumination inside the test section to view the bubbles clearly. It was only achieved when bright light was used through a third window from top. This caused more heating of the test section and the working fluid.

After facing several other practical problems with the aluminum test section, it was decided to discard the test section completely and design a whole new test section. To design a new test section the important criteria to consider were transparency and the ability to withstand the working temperatures and pressures. The plexiglass test section, which suited the criteria, was then designed.

Since a new TLC was required for every new set of test conditions, a permanently sealed test section was not an option. The real challenge was to design a leak proof test section which was very flexible so that it could be taken apart easily. For this reason, the test section was designed to have a main chamber that included a cube shaped top chamber and a bottom plate, to which the heater assembly was attached.

The top chamber, as shown in the Figure 4.1, was a cube with an internal volume of 60.9 x 60.9 x 66.4 mm made out of 5.1mm thick plexi glass.

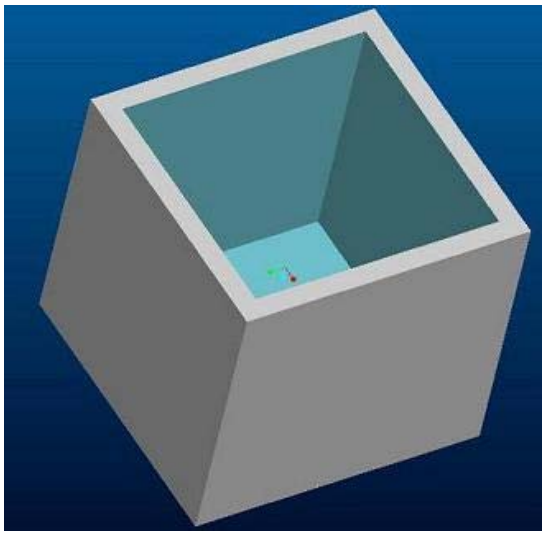

Figure 4.1: Top Chamber

A 90.1 x 102.6 mm plate machined out of 5.5 mm thick plexiglass, with attached TLC and heating element, as shown in Figure 4.2 was used as the bottom plate.

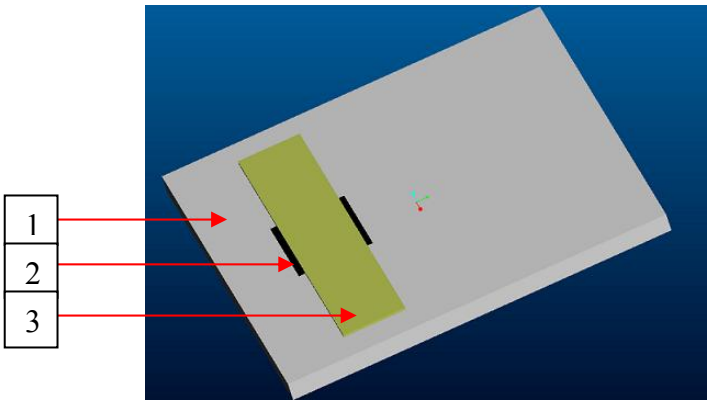

1. Bottom Plate
2. TLC sheet
3. Heating Element

Figure 4.2: Bottom plate and heating element

Initial experiments were run using a test section that was sealed using semi- permanent silicone glue that could be easily removed after the experiments. The bottom plate with heater assembly was glued to the top chamber. The test section was ready for the experiments after 24 hours of the working time of the glue. This test section worked well for sometime with no leaks. But during the progress of the experiments the constant supply of heat flux to the heating element resulted in the softening of the silicone glue. This eventually caused leakage and other problems.

In order to avoid the softening of the glue, it was decided to replace silicone and use epoxy. The bottom plate was glued to the top chamber using epoxy. But soon it was found that the vacuum, applied inside the test section caused its deformation as shown in Figure 4.3.

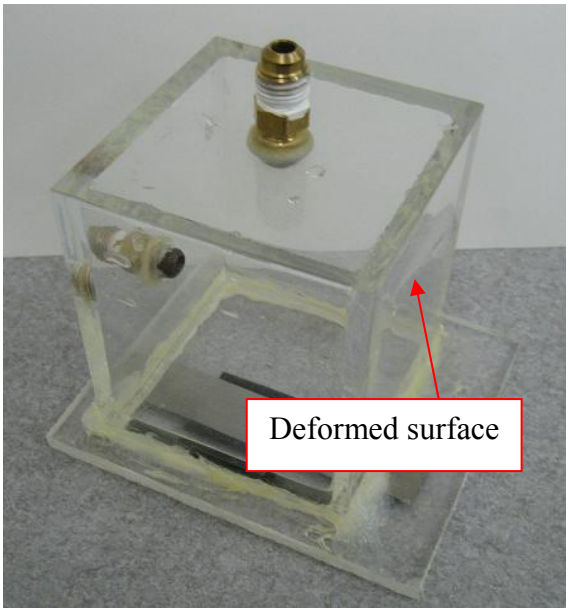

Figure 4.3: Deformed test section

After trying different glues it was concluded that the glue works only for a short period of time but not through out the experiment. All these attempts led to a flexible test section with quick grips, as shown in Figure 4.4.

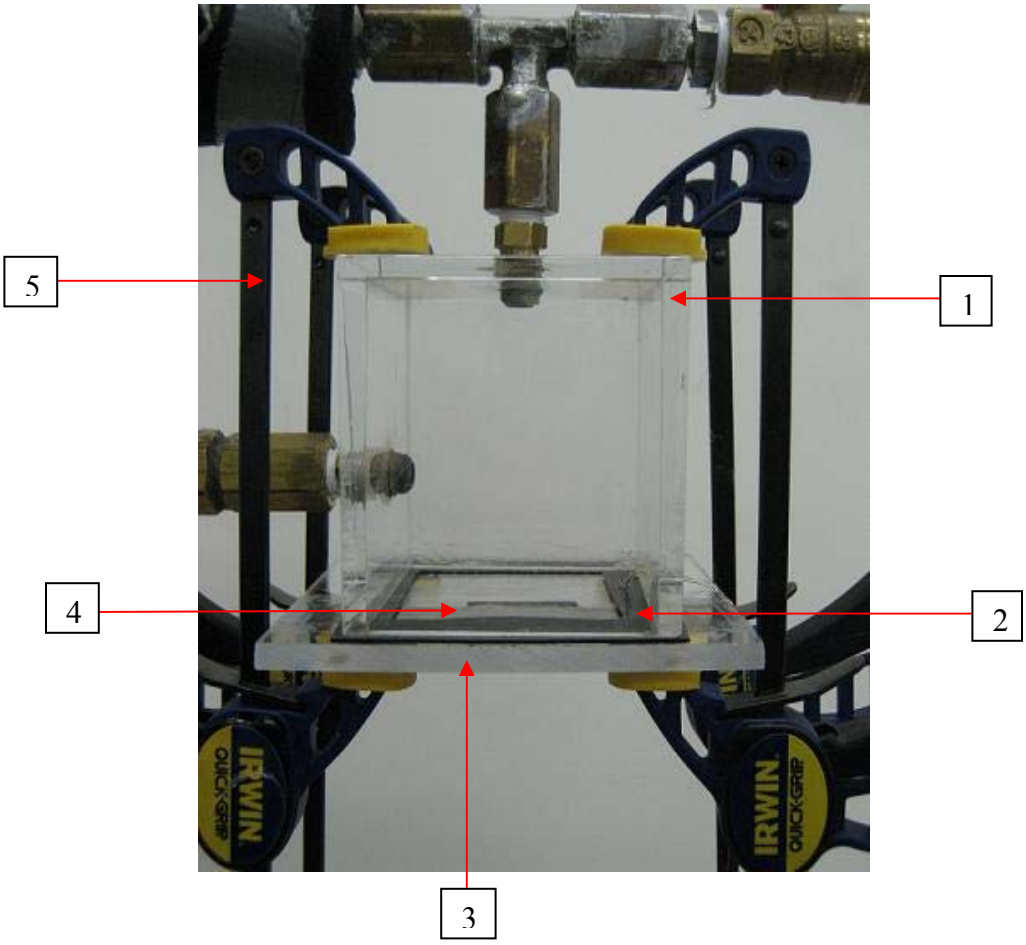

1. Top Chamber
2. Gasket
3. Bottom Plate
4. Heating Element
5. Quick Grip

Figure 4.4: Test section with quick grips

4.2.1.1 Main Chamber

The main chamber, as shown in Figure 4.4, had a top chamber and a bottom plate. The top chamber was provided with ports to supply water, to create vacuum and installation of measurement devices like pressure transducer and thermocouple. The bottom plate, with attached heating element and the top chamber were assembled together using a gasket and quick grips on the four corners. The quick grips were very easy to fix and remove.

The gasket was placed on the bottom plate and was pressed against the top chamber. The four quick grips were then placed loosely on each corner of the main chamber and the test section was adjusted in such a way that the camera system had the best possible view of both TLC and the heating element. Before running the experiment, the quick grips were tightly pressed to keep the test section stable and leak proof.

4.2.1.2 Working Fluid

Water was used as the working fluid in the current experimental study for the following reasons:

i. Dearth of experimental data for nucleate pool boiling in water at subatmospheric pressures.
ii. High heat of vaporization
iii. High thermal conductivity
iv. Non-toxic
v. Non-flammable

4.2.1.3 Heating Element

Fecralloy® (Fe 72.8/Cr22/Al4.8/Si0.1/Y0.3) was used as the heating element in the current experimental setup to boil water. This material was chosen because of its high electrical resistivity (134 μOhmcm). The liquid crystal thermography technique is limited to boiling on very thin walls, conditions that maximize the local variations in wall temperatures and minimize lateral conduction. For this reason 0.05mm thick Fecralloy® surface was used as a heating element. The standard foil of 2m in length and 180mm width from GoodFellow™ was cut in required dimensions and was used as the heating element.

4.2.1.4 TLC Sheet

TLC coated polyester sheets from HALLCREST™ were used to study wall temperatures. Standard sheets used a substrate of 125 micron clear polyester (Mylar). The sheets were printed on one side first with the micro encapsulated TLC coating, then with a black backing ink. The color change properties of the TLC coating were viewed through the clear, uncoated side of the sheet. TLC sheets with adhesive were found more suitable as the protective release-liner could be removed for easy adhesion to the flat surface of the heater. The sheets were of standard size 30cm x 30cm. The color change was from black to red, through the other colors of the visible spectrum to blue, with increasing temperature, and finally to black again. The TLCs, used in the experiments were:

1) R35C5W
2) R40C5W
3) R45C5W

RXC5W: Red start at X°C and Bandwidth = 5°C

4.2.2 Vacuum pump

The subatmospheric pressure was maintained inside the test section using an explosion proof vacuum pump (PX 100) from Precision.

Figure 4.5: Vacuum Pump

4.2.3 DC power supply

A high current DC regulated power supply was needed to provide the necessary heat flux. BK PRECISION regulated DC power supply (Model: 1794) with output of 0-30Volt and 0-30Amp was used in the present experiment to pass electrical current through the heating element to generate necessary heat flux.

Figure 4.6: DC power supply

4.2.4 Measurement devices

A pressure transducer and a thermocouple were used to measure pressure and temperature respectively, inside the test chamber. Temperature measurements were collected from E-type thermocouple, produced and calibrated by Omega Engineering™.

Figure 4.7: Pressure Transducer

OMEGA's PX209 series general purpose pressure transducer (PX209-015G5V, Pressure range: 0 to 15 psig and Output: 0 to 5 V dc) was used to make pressure measurements. These pressure

transducers were claimed to be accurate and highly reliable pressure transducers suitable for the harshest industrial environments. The small size and light weight of the PX209 series made them ideal for tough vibration and shock environments. The unusually high performance of this solid state pressure transducer came from the 4-active-arm bridge sensor using a micro-machined diffused silicon diaphragm and proprietary thin film media and dielectric isolation barriers.

The analog data from the thermocouple and pressure transducer was digitized using the National Instrument's temperature module (NI SCXI 1303) and pressure module (NI SCXI 1327) respectively. Both the modules were installed in the chassis (NI SCXI 1001).The data acquisition was monitored through out the experiment with the help of LABVIEW applications written for this project.

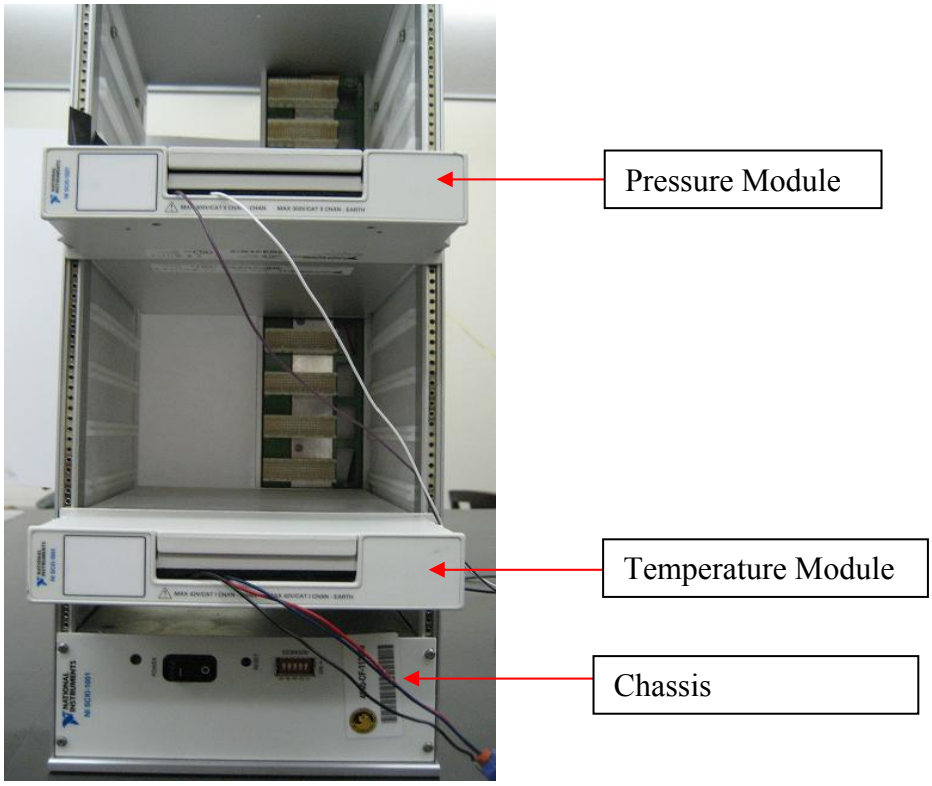

Figure 4.8: National Instruments' DAQ system

4.3 Experimental Procedure

A square shaped 20x20 mm TLC was cut from the standard TLC sheet and was glued on to the bottom plate using LOCTITE® silicone. The glue was chosen in such a way that it was transparent and did not cause any kind of contamination. Enough care was taken to avoid water from reaching the bottom of TLC. It was set to dry for sometime. Then the heater element was placed on top of the TLC and was attached to the bottom plate using the same silicone.

The top chamber was cleaned with cleaning liquid every time before and after the experiment. A gasket was placed in between the top chamber and the bottom plate, attached with heater assembly. The top chamber was positioned on the bottom plate in such a way that the distance of TLC tip from the wall of the top chamber was 5.6mm.They were held tight using quick grips. The test section was placed in the horizontal position. The CCD camera was placed underneath the test-section along with a frame grabber –PC set-up for capturing hue images through the plexi glass plate. A mirror arrangement, as shown in Figure 4.9, was placed next to the main chamber so that the same camera system records the growth of the bubble and its departure. Two light sources were used to illuminate the TLC coated surface for hue imaging and for recording the bubble dynamics on the nucleation site(s).The *in-situ* calibration, as explained in 4.3.1, was done to get the calibration coefficients.

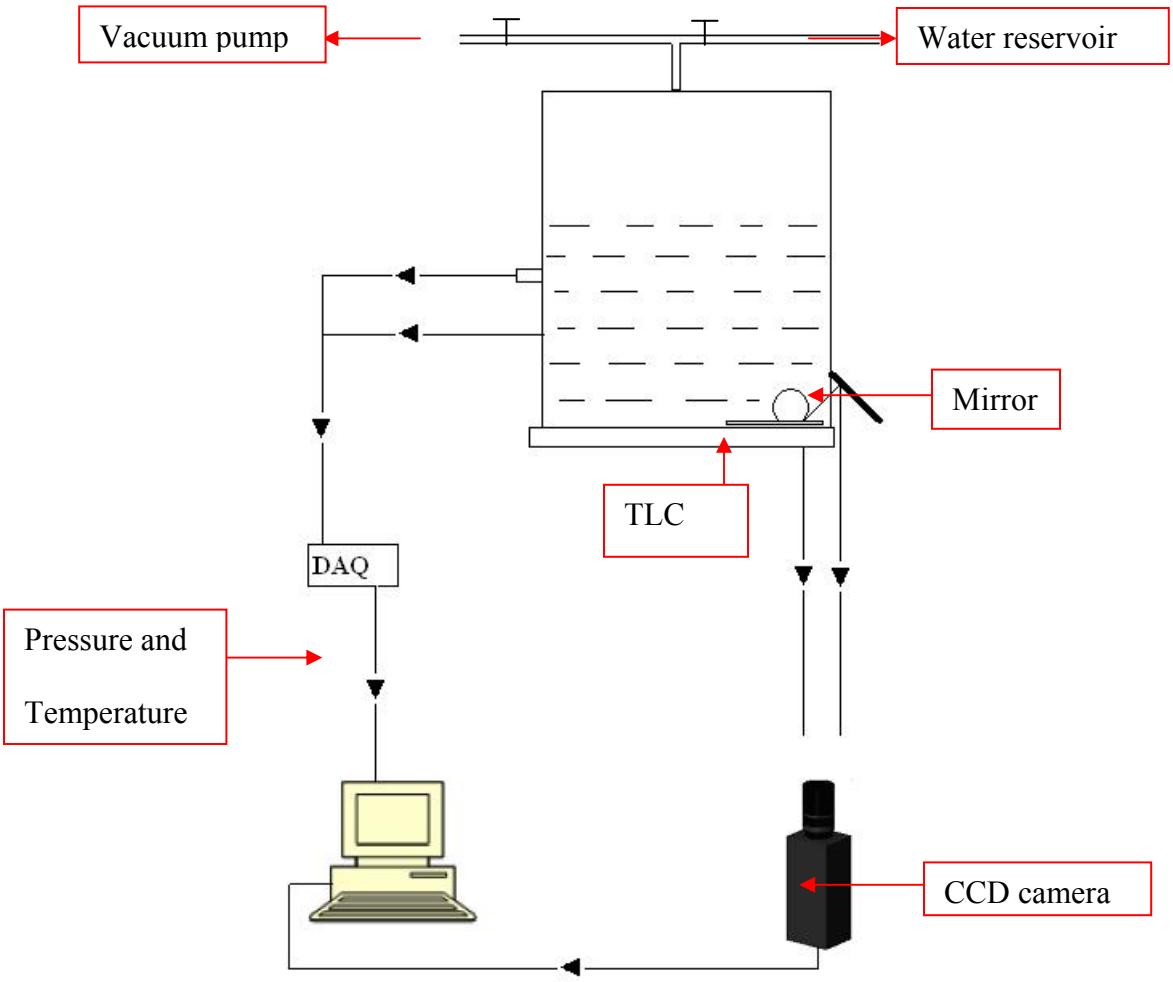

Figure 4.9: Pool boiling experiment and analysis systems

In order to run the actual boiling experiment at subatmospheric pressures, a very low constant pressure was maintained inside the main chamber, with working fluid inside by continuously running the vacuum pump. The pressure readings were constantly monitored using LabVIEW® application.

Electrical connections were made using copper strips along the two edges of the heating element. With this setup, the surface for TLC based temperature observation and the surface where nucleation occurred were on the opposite side of the heating element.

Using DC power supply, the surface of the heating element was heated to a temperature beyond the water saturation temperature at a particular test section pressure. Then CCD camera system was used to record the color play of TLC and the growth of the bubbles. The video files were digitized using the PC-RGB card and were stored as .vnm files using Coreco Imaging software. The .vnm files were converted to .avi files and then to individual frames. Each individual frame was analyzed using the software written for this project to get wall temperatures and the bubble dynamics.

As TLC hue capturing is sensitive to the angle of illumination as well as angle of viewing, enough care was taken to run the complete experiment without disturbing the experimental setup.

4.3.1 TLC Calibration

In order to use TLC for temperature measurement, hue *vs*. temperature relationship had to be first established through calibration. Since the response of TLC is extremely sensitive to the viewing angle and lighting conditions, calibration performed for a TLC painted surface is not necessarily valid for another. There can be significant differences in the response of the TLC even across a single surface. For this reason, it is always preferred to perform *in-situ* calibration and calculate the hue *vs.* temperature calibration curve for each pixel.

The TLC temperature bandwidth was selected so as to cover the expected variation in surface temperature during the experiments. During a calibration, the test-section was heated to a temperature beyond TLC bandwidth until it reaches the steady state as monitored by built-in thermocouple. The heating is then switched off and the test surface was allowed to cool.

Throughout the cooling process, the ROI temperature was monitored through a computer based data acquisition with thermocouple using LabVIEW® application written for temperature measurement. For every ΔT (~0.1°C) change in the surface temperature, a color image of the test surface was recorded. Calibration was done using the software written for this project. It automatically plotted the temperature of the TLC via thermocouple and hue value of the TLC, calculated from the RGB values of the individual pixels within an image.

The hue values and temperatures were plotted against each other and a regression equation was developed. This regression was only valid for the current experimental setup, which included lighting conditions and viewing angles.

Least squares regression was performed to fit a fifth order polynomial through the hue *vs.* temperature data. The calibration coefficients thus obtained were used to get the necessary wall temperature data from the images of TLCs recorded during the actual experiment, with the help of the software written for this project.

As the experiments were planned to be performed at different subatmospheric pressure test conditions, calibration was performed for each pressure test condition. Also calibration was performed at atmospheric pressure to check for pressure effects.

Calibration for the TLC (35-40°C) was done at two different pressures, atmospheric (101.32kPa) and working pressure (6.2 kPa). Both calibration curves were produced under identical lighting and ambient conditions. To calibrate the TLC, the test section was brought to 45°C and then slowly cooled while acquiring temperature and hue readings. The temperature was recorded using E-type calibrated thermocouple at 0.1°C intervals.

As shown in Figure 4.10, the two curves were almost identical only for a very narrow range of temperature (36-36.5°C). Otherwise they were different from each other with a maximum temperature difference of 0.6°C. Therefore, a universal curve could not be developed for all pressures. This made the *in-situ* calibration important.

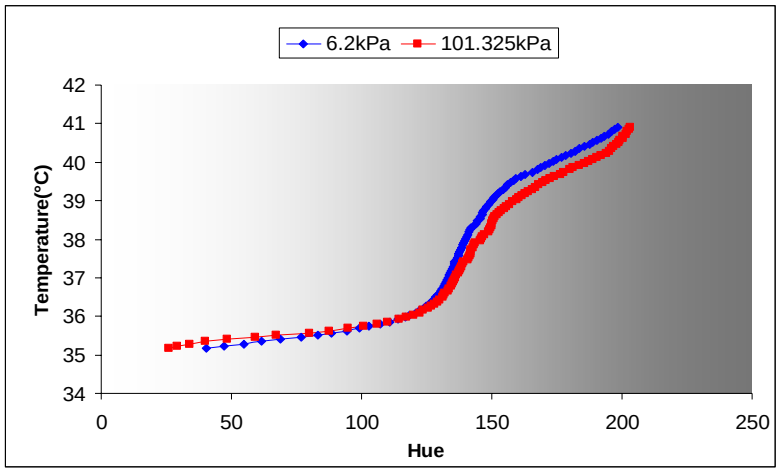

Figure 4.10: Calibration curves

4.4 Error Analysis

The calculation of errors in all measurements taken was based on information provided by the manufacturers of the measuring equipment. The voltage and current measured by the power supply had an error of ±0.2% ±10mV and ±0.5%±10mA, respectively. Electronic digital calipers used to measure the volume and thickness measurements had an uncertainty of ±0.02 mm. Based on these errors, standard deviation in heat flux was estimated as shown in Equation 4.1 and was found to be of the order of ±2.4%.

$$dq = \sqrt{\left(\frac{I}{A}dV\right)^2 + \left(\frac{V}{A}dI\right)^2 + \left(\frac{IV}{A^2}dA\right)^2} \qquad (4.1)$$

The conduction heat loss from the test section was very minimal during the experiments and it was found to be less than 5%.The pressure transducer used for pressure measurements had an accuracy of 0.25% FS (including linearity, hysteresis and repeatability). When temperature was determined from hue value by using the polynomial curve fit, the uncertainty expected for a single pixel could be calculated from the procedure presented by Hay and Hollingsworth [10].

$$\delta T = \left[\left(\frac{dT}{dh}\delta h\right)^2 + \left(2.SSE\right)^2\right]^{\frac{1}{2}} \quad , \qquad (4.2)$$

where dT/dh is the slope of the curve fit. The standard estimate of error, SEE, is used as a descriptor of the scatter of the mean h values about the curve fit and is defined as

$$SSE \equiv \left[\sum_{i=1}^{k}\left(T_i(h) - T_{fit,i}(h)\right)^2 / (k - j - 1)\right]^{\frac{1}{2}} \qquad (4.3)$$

where k is the number of data points and j is the order of the curve fit. The uncertainty in temperatures estimated from Equations (4.2), (4.3) and from thermocouple was ±0.3°C.

CHAPTER 5 RESULTS AND DISCUSSION

The nucleate pool boiling experiments are conducted in water under subatmospheric pressures at saturation temperature. The study is carried out for four different test conditions as shown in the Table 5.1.

The natural roughness of the surface is used to produce bubbles. The bubble growth is studied for these test conditions on a horizontal flat surface using both the images of the bubble and the synchronized two-dimensional surface temperature data from TLC images.

Table 5.1: Experimental conditions

EXPERIMENT	P_∞(kPa)	q" (kW/m^2)
Case I	6.2	1.88
Case II	6.2	2.70
Case III	8.0	2.70
Case IV	8.0	3.66
Case V	8.0	4.50

In this chapter, surface temperature data and images of the bubbles for one test condition ($P\infty$ = 6.2kPa and q" = 1.88 kW/m^2) are presented and the processing procedure of the data to determine characteristics of the nucleation process is described. This chapter also includes a summary of the results for the remaining conditions and a discussion of the relevant differences between the cases.

5.1 Bubble Growth

An isolated bubble has been analyzed from inception to lift-off from the surface. Figure 5.1 shows a sequence of actual images describing a single ebullition cycle for water under subatmospheric pressure (6.2kPa).

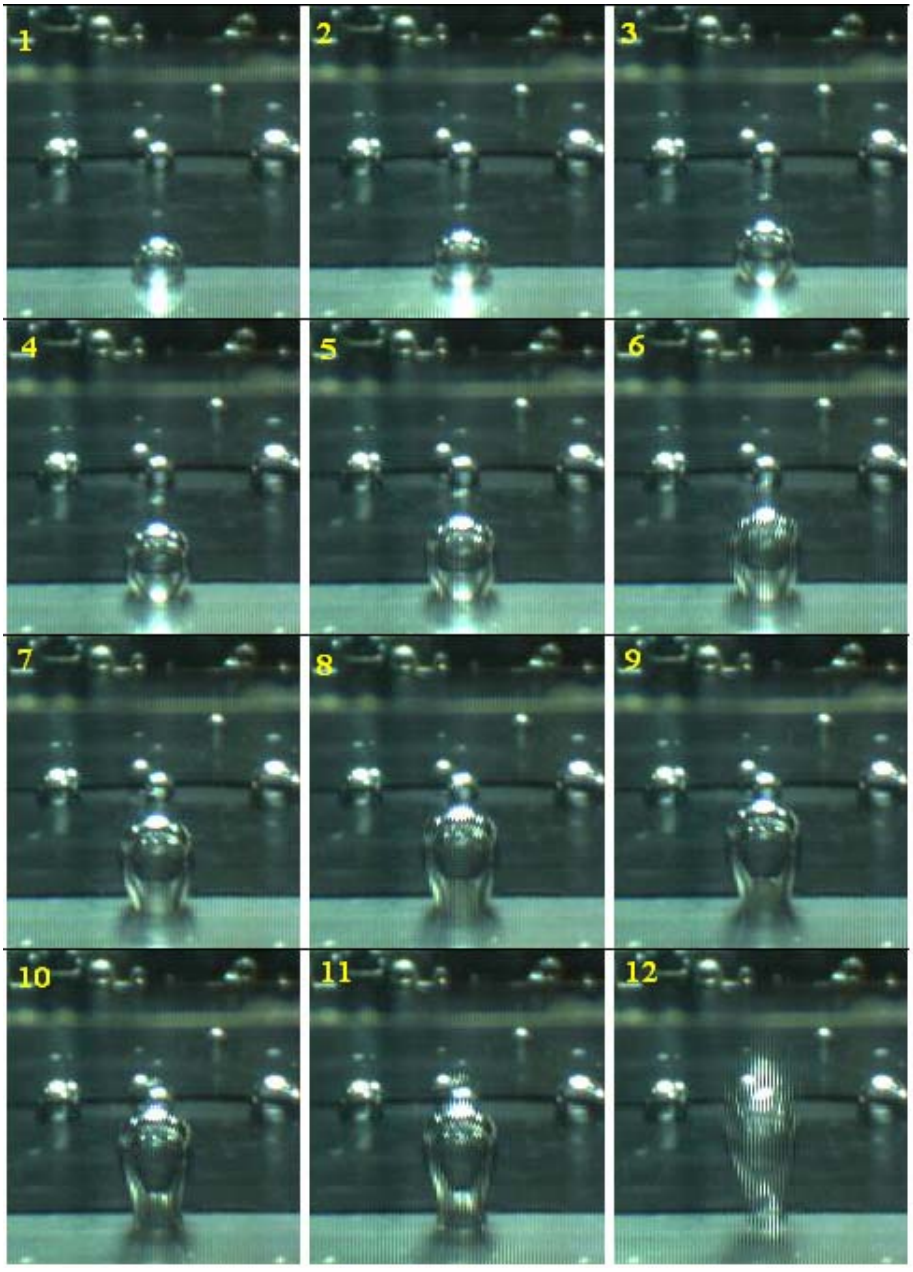

Figure 5.1: A bubbling event for Case I (time interval: 1/30 sec)

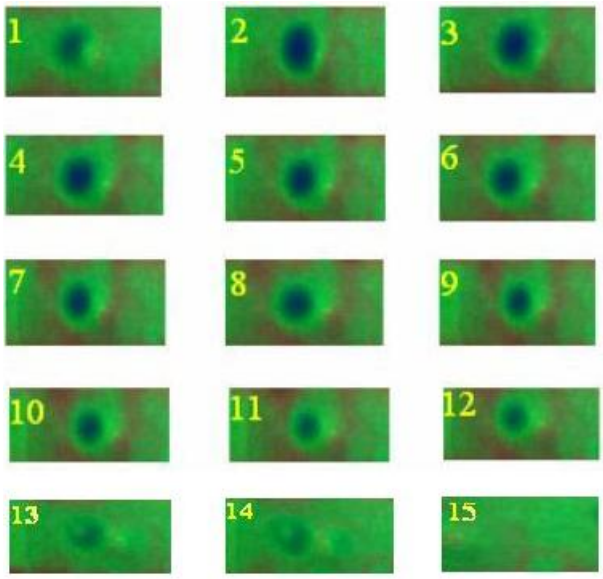

Figure 5.2: Corresponding TLC image set during the bubbling event

Initially the nucleus is surrounded by relatively cool liquid at T∞. As time goes on, the liquid is warmed by heat transfer from the surface, and the nucleus begins to grow when the liquid temperature exceeds the vapor temperature over the entire liquid-vapor interface.

Figure 5.1 represents twelve consecutive images from t = 33.33ms through t = 399.99ms and the corresponding TLC images are shown in Figure 5.2. Following nucleation, the bubble initially grows rapidly faster than 1/30 sec through the superheated liquid boundary layer and removing this layer locally from the wall (Frame 1 of Figure 5.1). The resulting rapid growth of the bubble is primarily resisted by the inertia of the liquid and the growth rate gradually diminishes in the later stages. For this inertia-controlled early stage of the bubble growth process, the bubble grows in nearly hemispherical shape (Frame 1-3 of Figure 5.1).

During the bubble growth, a thin liquid film is left under the growing bubble as a result of the very high viscous stress in the liquid near the wall. Since this liquid film is immediately adjacent to the hot wall, it represents the highest liquid surface temperature to which the bubble is exposed. Hence, more mass evaporates into the bubble, allowing the bubble to grow. It is observed that at subatmospheric pressures the contribution of the evaporation microlayer (at the base of the vapor bubble) is greater when compared to that of the relaxation microlayer (surrounding a part of the bubble dome). During the bubble growth, evaporation microlayer beneath the bubble evaporates, starting at the center, where a 'dry spot' occurs at the heating surface. The formation of the little blue spot in the corresponding TLC image (Figure 5.2 (1)) indicates that the evaporation of microlayer has just begun at the center of the bubble. The analyzed temperature data is in agreement with the above statements. This is discussed in greater detail in section 5.3.

At subatmospheric pressure, the vapor bubbles originating at the superheated wall are observed to have the shape of a hemisphere during the initial stage (Frame 1 - 2 of Figure 5.1). The bubble is expanded by an excess pressure corresponding to the boundary superheating and bubble growth is governed by inertia.

At later stages of the bubble growth a neck is observed close to the wall where the bubble is attached (Frames 8 through 11 of Figure 5.1). The possible reason for the neck formation is that the balance of hydrostatic pressure distribution and surface tension over the height requires that the sum of the curvatures increase with distance from the top of the bubble. For slow growth

rates the shape of the bubble is defined by Equation 5.1. External pressure on the bubble varies hydrostatically and internal pressure is constant.

$$\rho g z + P_v - P_0 = \sigma \left(\frac{1}{r_1} + \frac{1}{r_2} \right) \tag{5.1}$$

Where P_0 is the absolute pressure at the top of the bubble, Pv is the internal pressure and z is the height of the bubble from its top and σ is the surface tension. From Equation 5.1, it is noted that as z increases the sum of the curvatures ($1/r_1 + 1/r_2$) increases, everything else being constant. This implies that when there is an increase in r_2, the radius of curvature in the vertical direction, the sum of the curvatures increases only if there is a decrease in r_1, the radius of curvature in the horizontal direction. This explains the formation of the neck close to the wall where the bubble is attached.

The neck formation is observed only in the case of large bubbles but not small bubbles. Since the pressure difference between internal and external pressure is much larger than hydrostatic pressure in the case of small bubbles, they are spherical in shape.

Once the neck forms on the wall, where the bubble is attached, it starts to elongate with the growth of the vapor bubble (Frames 8-11 of Figure 5.1). The height of the bubble increases with time and accelerates the water ahead of the bubble. When the height of the bubble stops to grow, it results in the deceleration of the water. This decelerated water produces a negative pressure on the top, changing the shape of the bubble and affects neck, causing it to reduce in size and eventually close the neck (Frames 11-12 of Figure 5.1).

In summary, after inception, the bubble shape is a spherical sector which expands with time. The shape changed from spherical to vertical elongation with the height greater than the width and then to a neck. Soon after the neck appeared, the bubble center accelerated upward and the stretching of the neck extended until the time of detachment.

One of the important observations made in this experimental study is that the formation of the neck at the later stages of the bubble growth is observed only in the case of lower subatmospheric pressure and heat flux because of the larger bubble size.

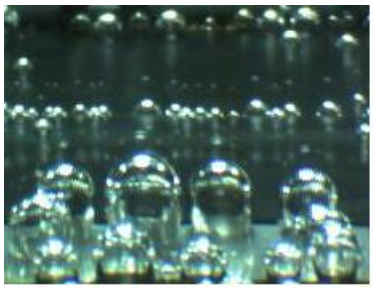

Figure 5.3: Nucleation sites at high heat flux

It was observed during the experiments that the number of active nucleation sites increased with an increase in heat flux, as shown in Figure 5.3.

5.2 Analysis of the Temperature Data

The TLC images in Figure 5.2 are processed using the software written for this project and the temperature data is analyzed and compared with the corresponding bubble images in Figure 5.1. The important observation of this present study is the formation of 'dry spot' beneath the vapor bubble. From visual comparison of Figure 5.1 and Figure 5.2, it is clearly seen that the intensity

of the blue spot gradually increases during the bubble growth and fades away at the detachment of the bubble.

The temperature difference across the evaporation microlayer leads to a heat flow through this layer. As a consequence, the layer evaporates, beginning at the center (Figure 5.2 (1)), where the layer has the smallest initial thickness and is generated at an early instant. This evaporation results in the formation of 'dry spot' causing the local temperature of the wall to reach its maximum value. The increasing trend in the wall temperature continues until the microlayer evaporates completely.

Since, the heating element under the bubble is now in contact with the vapor but not the liquid, further heating of the wall results in an increase in the intensity of the dry spot (Figure 5.2 (2)-(8)). The contact area of the bubble with the heating element starts to recede after reaching a maximum value and the rewetting takes place. Therefore, the intensity of the dry spot gradually decreases and fades away at the detachment (Figure 5.2 (9)-(12)).

Detailed wall temperatures are obtained for a 8mm x 8mm region on the heated surface at and near the growing bubble (Frame 8 of Figure 5.1).The 3-dimensional plot of measured temperatures from the corresponding TLC image (Figure 5.2 (8)) is shown in Figure 5.4.

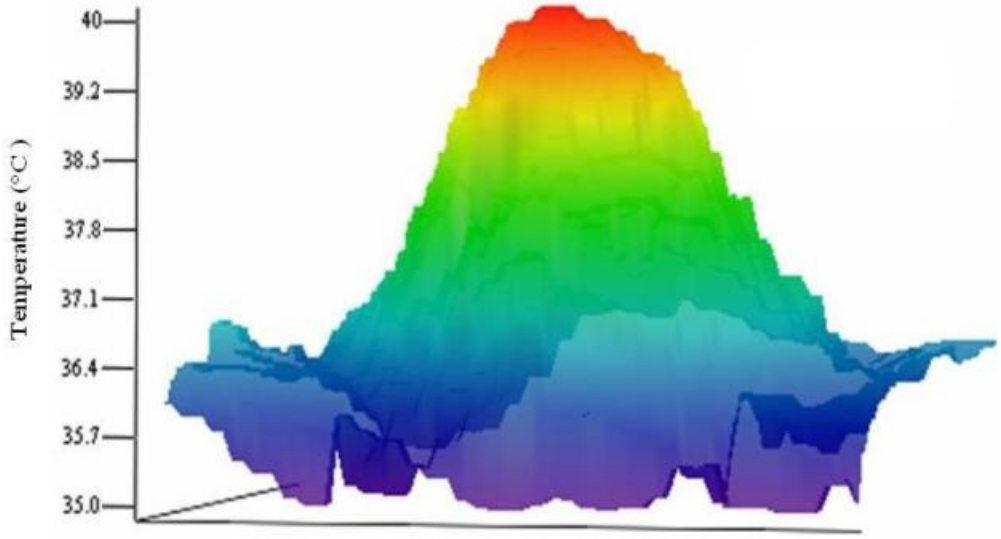

Figure 5.4: 3-D Temperature contour

As shown in Figure 5.4, the wall temperature is at its peak at the very center of the bubble and it starts to decrease radially away from the center of the bubble. The existence of the dry spot under the bubble is clearly evident from the 2-D temperature contour plot, as shown in Figure 5.5.

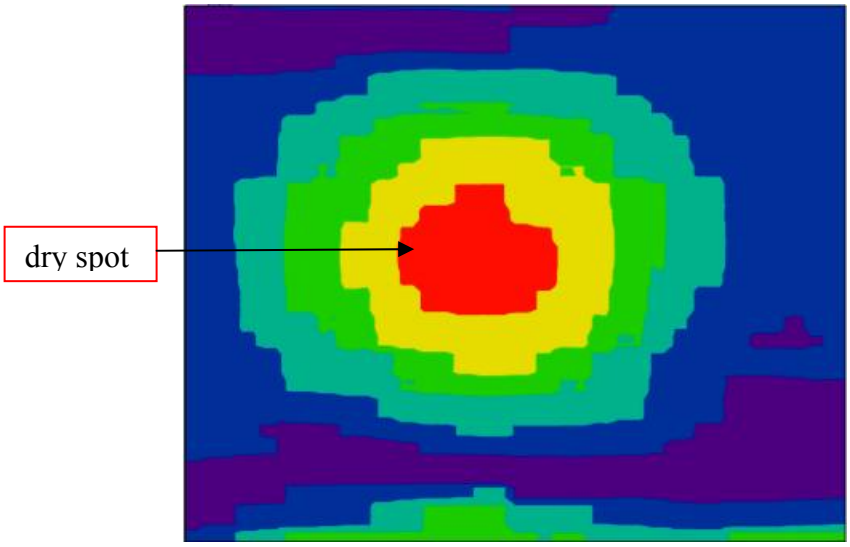

Figure 5.5: 2-D Temperature contour

The time variation of local temperature during the bubbling event (Figure 5.1) is shown in Figure 5.6. The average local temperature at the bubble (Frame 1 of Figure 5.1) is 37.9°C and it increases in the next two frames reaching 39.4°C. At later stages of the bubble growth, a decrease in temperature is observed. This is explained by the fact that during the bubble growth, the apparent contact line of the vapor bubble with the wall starts to recede soon after reaching a maximum value. This causes the receding liquid to rewet the dried out wall. The temperature decreases further at detachment of the bubble.

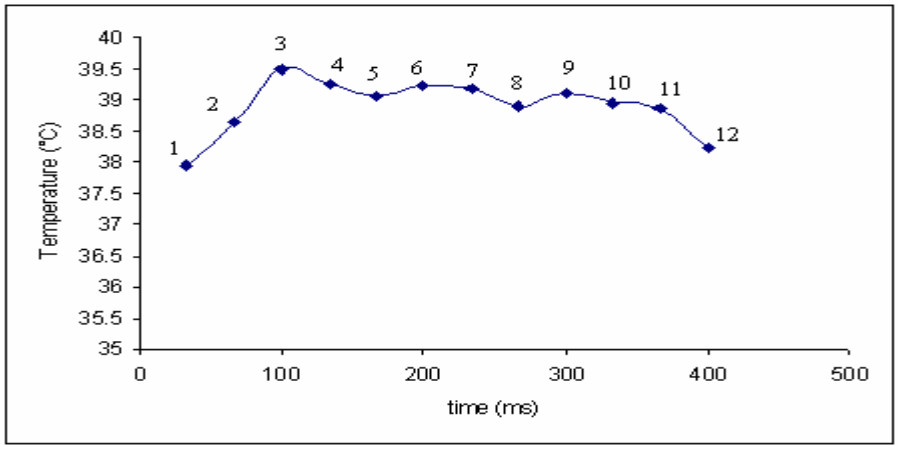

Figure 5.6: Time variation of the local temperature

The local temperature data, during the bubbling event is plotted against the distance from the center of the bubble, as shown in Figure5.7. It is noted that the local temperature of the wall is at its peak at the center of the bubble and it varies from 38.6°C to 39.7°C.

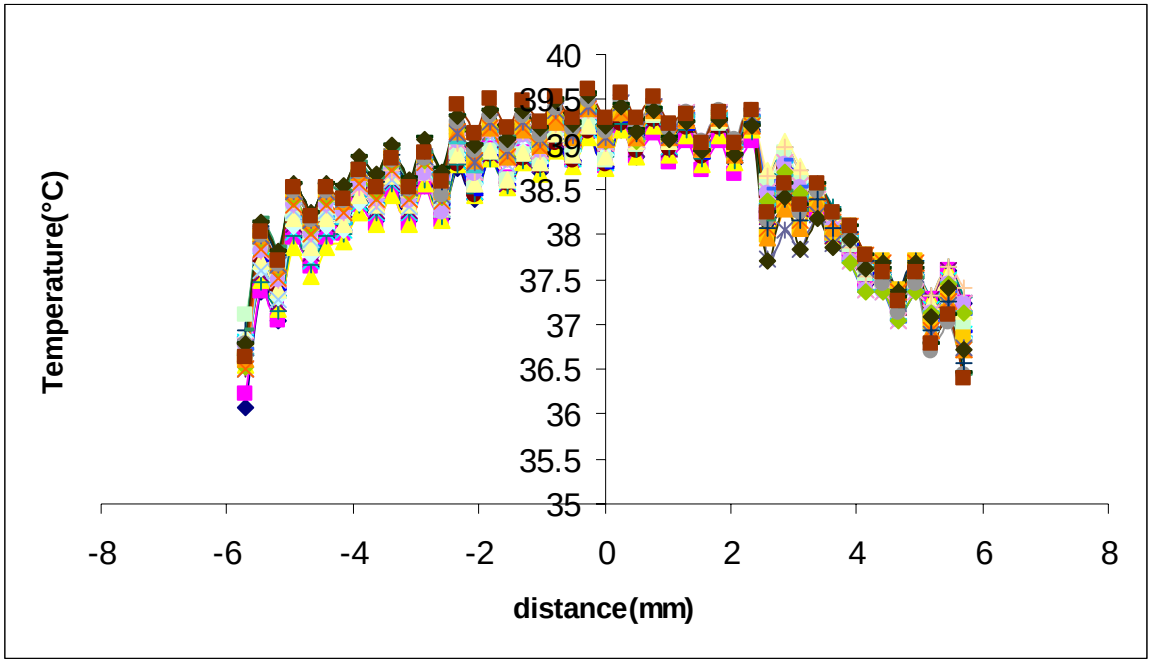

Figure 5.7: Variation of wall temperature beneath the bubble

5.3 Bubble Image Processing

The bubble images are analyzed using software written for this project. This takes the profile of the bubble perimeter with an accuracy of ±1 pixel. In order to characterize single bubble dynamics quantitatively, the bubble size in each frame of the digitalized video is obtained using the software.

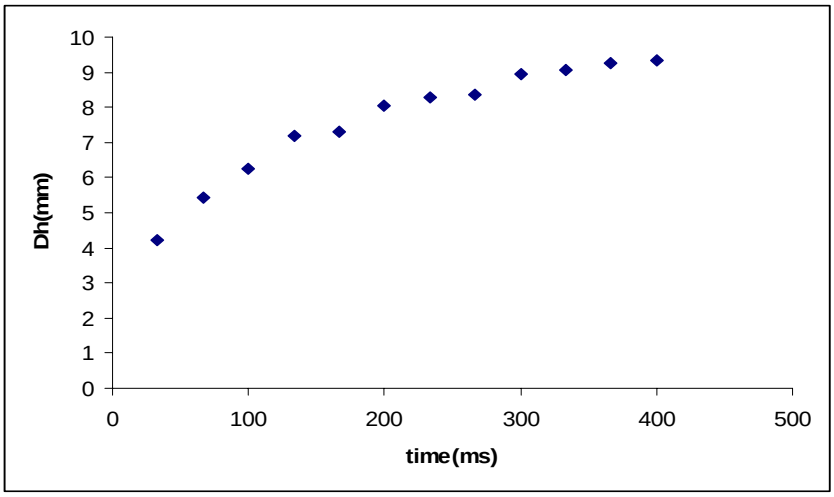

Figure 5.8: Time variation of bubble diameter

The hydraulic diameter of the vapor bubble beginning from the inception to its departure is plotted against the time. As can be seen in Figure 5.8, since, the growth rate gradually diminishes; the slope of a growth curve decreases with increasing time up to departure. The bubble frequency for different bubbles at these experimental conditions is of the order of 2.5-3.6 Hz.

The diameter of the contact area of the vapor bubble and the heating wall is plotted against time in Figure 5.9. It is observed from this figure that value of the contact diameter increases first reaching a maximum value and then it starts to decrease owing to the contraction of the bubble area, necking, resulting in the departure of the bubble.

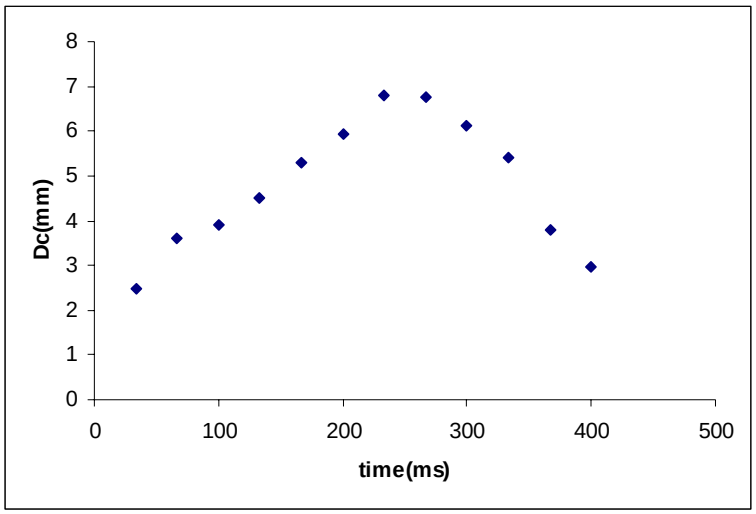

Figure 5.9: Time variation of Diameter of contact area

From Figure 5.10, it can be seen that the maximum height of the vapor bubble from the heated wall increases with time reaching a maximum value of 9.8mm, just before the departure. Formation of the neck and its elongation results in the greater values of the height.

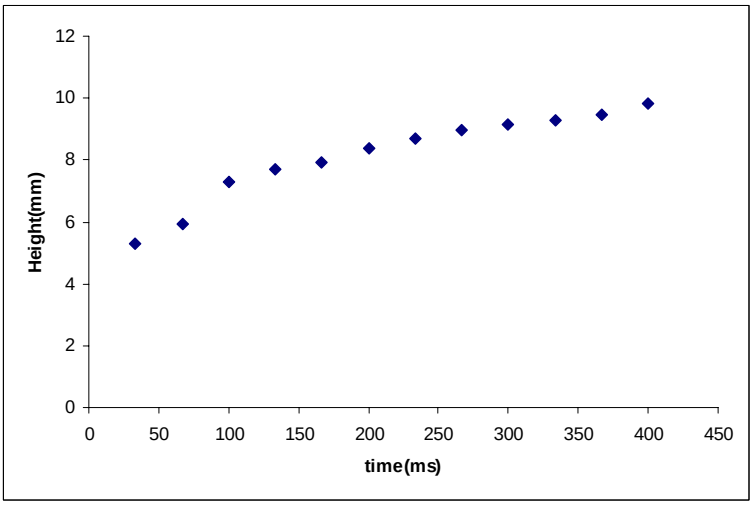

Figure 5.10: Time variation of bubble height

5.4 Experimental Results at Different Test Conditions

CASE II: q" =2.70 kW/m^2 P = 6.2kPa

The experiment is run at the same subatmospheric pressure as in case I, but at a higher heat flux. Experimental data representing one complete bubble cycle for this case is summarized in Figure 5.10. The temperature at the center of the bubble, as shown in Figure5.11 (a) is varied from 42.5°C to 43.7°C. The hydraulic diameter, D_h, starting from 4.03mm increased to a maximum value of 8.62mm just before the departure. From Figure5.11 (b), it is noted that the slope of the curve, D_h *vs* time, followed the same trend as in the previous case.

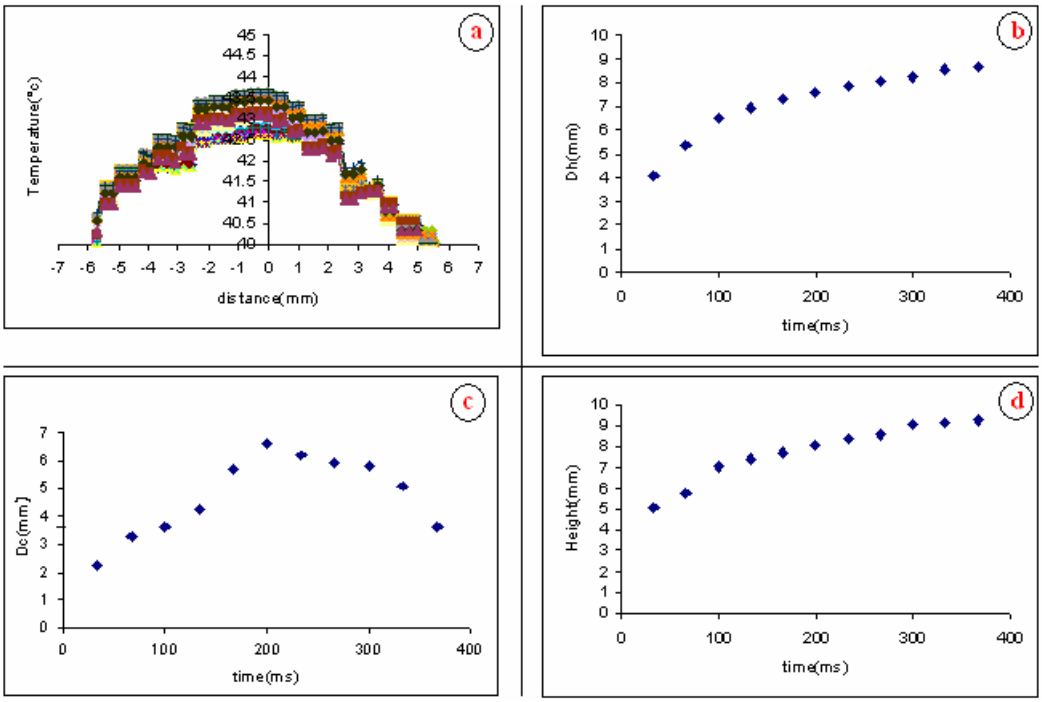

Figure 5.11: Experimental results for case II

Following the nucleation, the contact diameter, D_c, of the bubble increased to a maximum value of 6.62mm staring from 2.26mm, as shown in the Figure 5.11 (c), and decreased to 3.61mm just before the departure of the bubble. The height of the bubble, as shown in Figure 5.11(d), reached to a maximum value of mm starting from 9.23mm. It is also observed that the bubble frequency is of the order of 2.7 to 3.9 Hz. Therefore, a decrease in departure diameter and an increase in bubble frequency are observed in comparison to case I.

<u>CASE III</u>: q" = 2.70 kW/m^2 P = 8.0kPa

The experiment is run at the same heat flux as in case II, but at a slightly higher subatmospheric pressure. Figure 5.12 summarizes the Experimental data representing a complete bubble cycle.

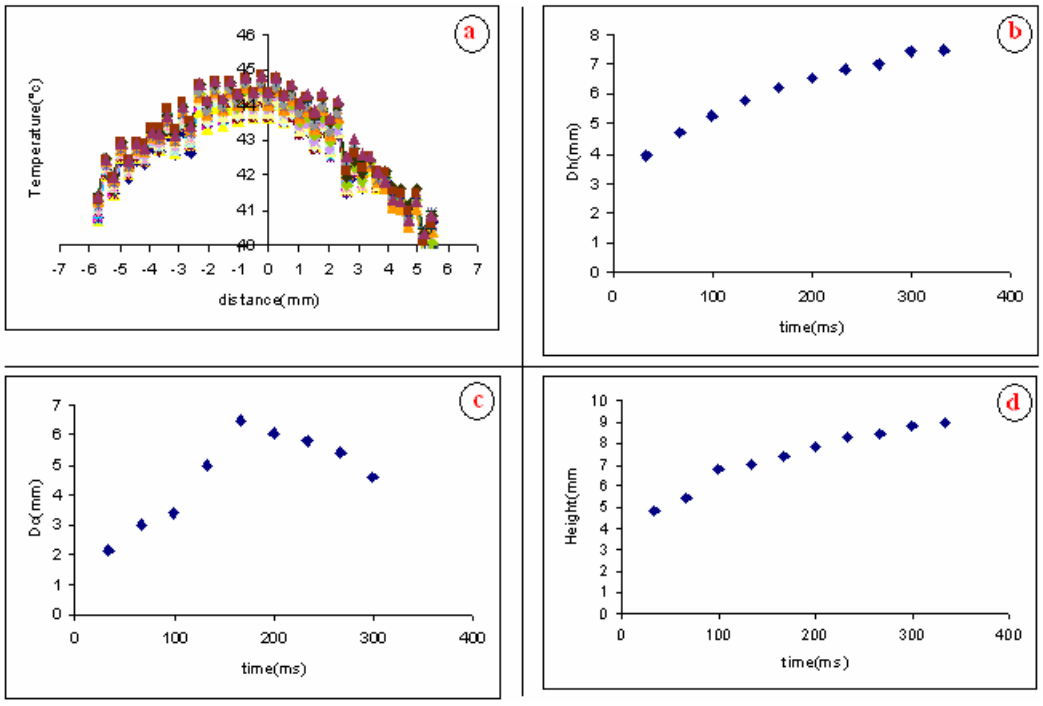

Figure 5.12: Experimental results for case III

The temperature at the center of the bubble, as shown in Figure5.12 (a) is varied from 43.3°C to 45.0°C. The hydraulic diameter, D_h, starting from 3.9mm increased to a maximum value of 7.46mm just before the departure. From Figure5.12 (b), it is noted that the slope of the curve, D_h *vs* time, followed the same trend as in the previous case. Following the nucleation, the contact diameter, D_c, of the bubble increased to a maximum value of 6.47mm staring from 2.14mm, as shown in the Figure 5.12 (c), and decreased to 4.6mm just before the departure of the bubble. The height of the bubble, as shown in Figure 5.12(d), reached to a maximum value of 8.96mm starting from 4.84mm. It is also observed that the bubble frequency is of the order of 3.1 to 4.2 Hz. Therefore, a decrease in departure diameter and an increase in bubble frequency are observed in comparison to case II.

<u>CASE IV</u>: q"= 3.66 kW/m^2 P =8.0kPa

The experiment is run at a higher heat flux and same subatmospheric pressure as case III. Figure 5.12, represents experimental data for one complete bubble cycle for this case. The temperature at the center of the bubble, as shown in Figure5.13 (a) is varied from 47.8°C to 49.4°C. The hydraulic diameter, D_h, starting from 3.84mm increased to a maximum value of 6.92mm just before the departure. From Figure5.13 (b), it is noted that the slope of the curve, D_h *vs* time, followed the same trend as in the other cases.

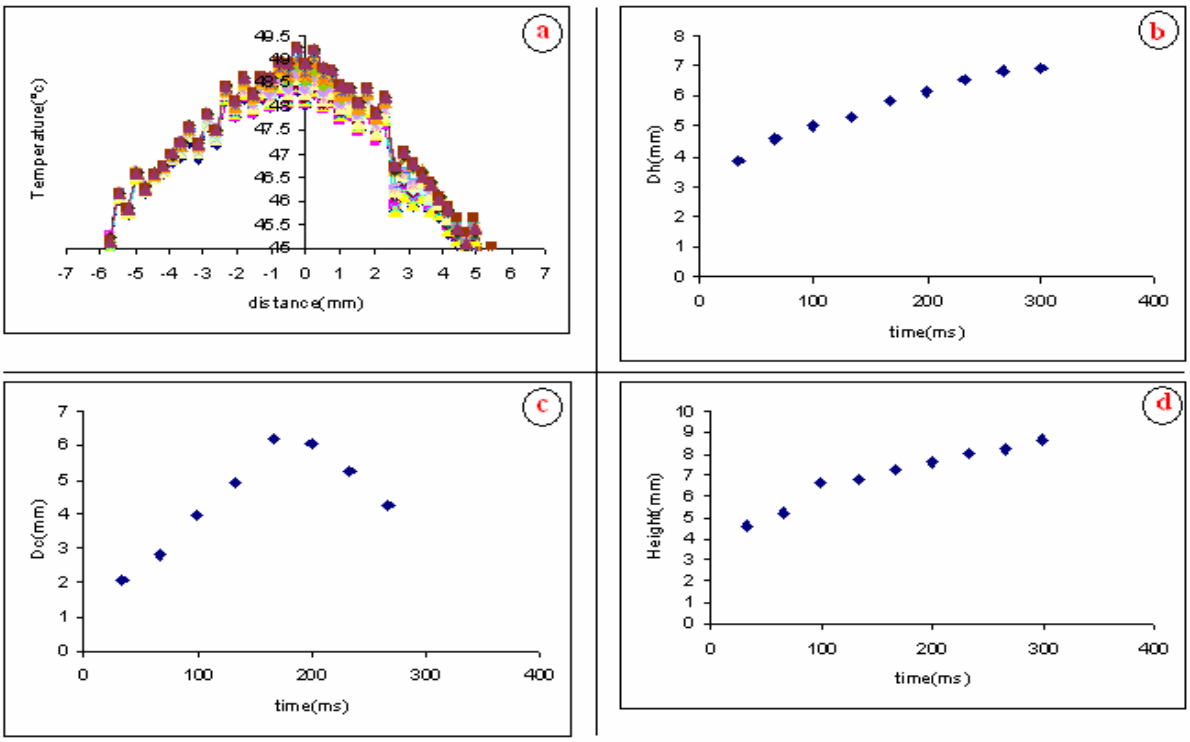

Figure 5.13: Experimental results for case IV

Following the nucleation, the contact diameter, D_c, of the bubble increased to a maximum value of 6.20mm staring from 2.06mm, as shown in the Figure 5.13 (c), and decreased to 4.2mm just before the departure of the bubble.

The height of the bubble, as shown in Figure 5.13(d), reached to a maximum value of 8.64mm starting from 4.61mm. It is also observed that the bubble frequency is of the order of 3.3 to 4.9 Hz. Therefore, a decrease in departure diameter and an increase in bubble frequency are observed in comparison to case III.

CASE V: q"= 4.50 kW/m^2 P =8.0kPa

The experiment is run at a higher heat flux and same subatmospheric pressure as case IV. Figure 5.14, represents experimental data for one complete bubble cycle for this case. The temperature at the center of the bubble, as shown in Figure5.14 (a) is varied from 48.1°C to 49.7°C. The hydraulic diameter, D_h, starting from 3.64mm increased to a maximum value of 6.44mm just before the departure. From Figure5.14 (b), it is noted that the slope of the curve, D_h *vs* time, followed the same trend as in the other cases.

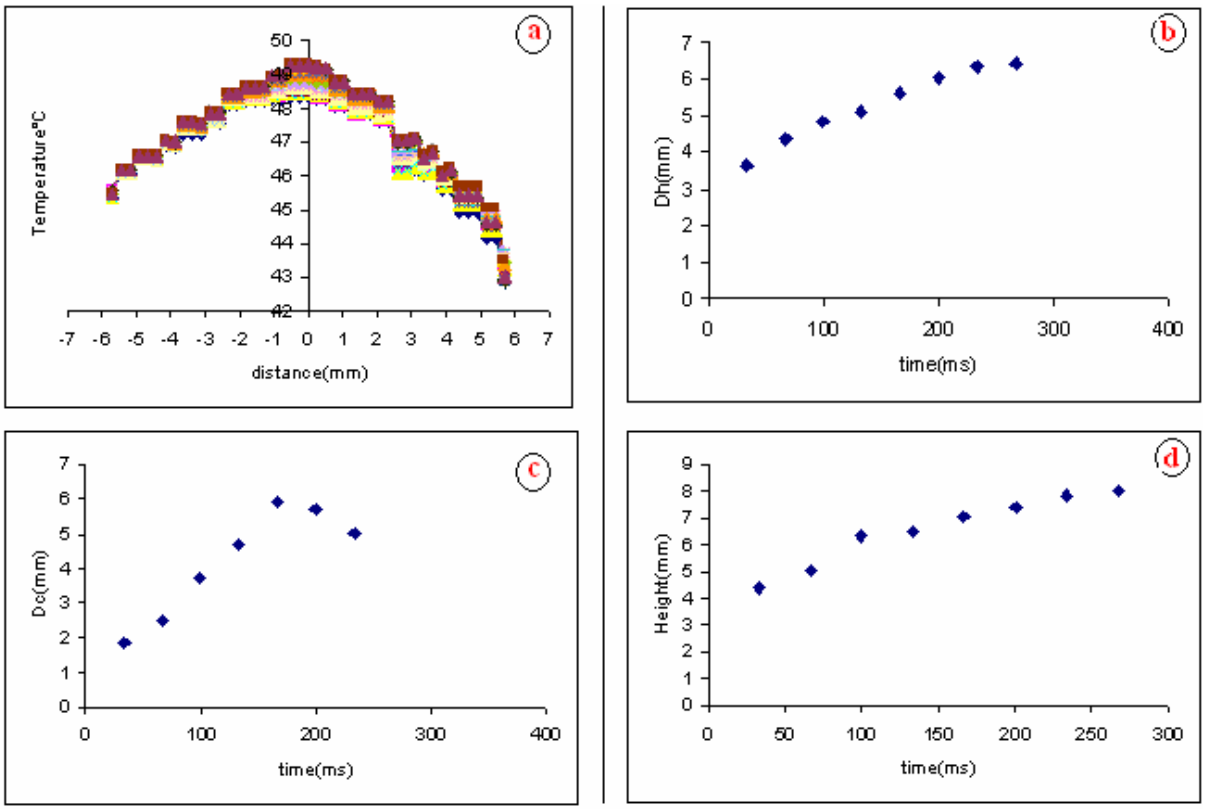

Figure 5.14: Experimental results for case V

Following the nucleation, the contact diameter, D_c, of the bubble increased to a maximum value of 5.92mm staring from 1.86mm, as shown in the Figure 5.14 (c).

The height of the bubble, as shown in Figure 5.14(d), reached to a maximum value of 8.01mm starting from 4.41mm. It is also observed that the bubble frequency is of the order of 3.7 to 5.4 Hz. Therefore, a decrease in departure diameter and an increase in bubble frequency are observed in comparison to case IV.

CHAPTER 6 CONCLUSIONS AND FUTURE WORK

6.1 Conclusions

A preliminary experimental study was done to investigate the use of Liquid Crystal Thermography and image processing techniques in nucleate pool boiling experiments. This study provided experimental data and enabled characterization of bubble dynamics during the heterogeneous nucleation process of water at subatmospheric pressures.

The experiment was started by heating the surface at required operating conditions with passage of electrical current through the copper strips. During the experiment, Ebullition cycles were captured using the camera system for different test conditions. Thousands of images, with TLCs and corresponding bubble growth were recorded using a 3 CCD camera system. These images were then processed using different modules of the software written for this project and the data was analyzed.

Based on the experimental results obtained, the following conclusions are derived:

- The thin liquid evaporation microlayer between the bubble and the heating wall evaporates gradually, starting at the center. Eventually, a dry spot forms beneath the bubble. This phenomenon is significant in the case of boiling at subatmospheric pressure, and has been captured in detail in this study.
- At constant heat flux, increasing the system pressure results in the increase of bubble frequency and a decrease in the bubble departure diameter.

- At constant system pressure, increasing the heat flux results in the increase of bubble frequency and a decrease in the bubble size.
- Number of the active nucleation sites was seen to increase with an increase in the heat flux at constant subatmospheric pressure.
- The formation of neck at the later stages of the bubble growth is observed only in the case of lower subatmospheric pressure and heat flux because of the larger bubble size.

6.2 Future Work

The pool boiling facility designed for this study can be used to run experiments with other working fluids, depending on the compatibility of the liquid with the materials of the test section. It is possible to obtain experimental data for a wide range of test conditions.

The following recommendations are made to improve the current experimental setup:

- A high-end camera system with better spatial and temporal resolution can be used to get more accurate data.
- TLCs with higher band width can be used to avoid the frequent replacements of TLCs.
- Mirror arrangement can be replaced by two identical camera systems to get the synchronized data.
- Materials with different electrical resistivities can be used as heating elements in these experiments to get more experimental data.
- Materials with known surface roughness can be used as heating elements to study the nucleation cavities.

REFERENCES

1. Mary Anne White, Monique LeBlanc., (1999). "Thermochromism in Commercial Products" Journal of Chemical Education Vol.76 No.9.
2. J.A. Stasiek, T.A. Kowalewski.,(2002). "Thermochromic liquid crystals applied for heat transfer research" OPTO-ELECTRONICS REVIEW 10(1), 1-10.
3. Bosnjakovic, F. (1930). "Verdampfung und Flussigkeitsuberhitzung." Tech. Mech. Thermodyn. Bevl. **1**: 358-362.
4. Fritz, W., and Ende, W. (1936). "Verdampfungsvorgang nach Kinematographischen Aufnahmen und Dampfblasen." Phys. Z. **37**: 391.
5. Forester, H. K., and Zuber, N. (1954). "Growth of Vapor Bubbles in Superheated Liquid." J. Appl. Phys. **25**: 474- 478.
6. Plesset, M. S., and Zwick, S. A. (1954). "The Growth of Vapor Bubbles in superheated Liquids." J. Appl. Phys. **25**: 493- 500.
7. Johnson, M. A., De La Pena, J., Mesler, R. B. (1966). "Bubble Shapes in Nucleate Boiling." AIChE J. **12**: 344-348.
8. Griffith, P. (1958). "Bubble Growth Rates in Boiling." J. Heat Transfer. **80**: 721-726.
9. Savic, P. (1958). "Discussion on Bubble Growth Rates in Boiling." Int. J. Heat Mass Transfer. **80**: 726- 728.
10. Bankoff, S. G., Mikesell, R. D. (1958). "Growth of Bubbles in Liquid of Initially Non uniform Temperature". ASME Meeting Nov 30-Dec 5: 58-A105.
11. Cole, R., and Shulman, H. L. (1966). "Bubble Departure Diameters at Subatmospheric Pre ssures." Eng. Prog. Symp. Ser. **62**(64): 6-16.
12. Mikic, B. B., and Rohsenow, W. M. (1969). "Bubble Growth Rates in Non-Uniform Temperature Field," Prog. Heat Mass Transfer. **2**: 283-292.
13. Cooper, M. G., and Lloyd, A. J. P. (1969). "The Microlayer in Nucleate Pool Boiling." Int. J. of Heat Mass Transfer. **12**: 895-913.
14. Van Stralen, S. J. D., Sohal, M. S., Cole, R., and Sluyter, W. M. (1975). "Bubble Growth Rates in Pure and Binary Systems: Combined Effect of Relaxation and Evaporation Microlayers." Int. J. Heat Mass Transfer. **18**: 453-467.

15. Hsu, S. T., and Schmidt, F. W. (1961). "Measured Variations in Local Surface Temperatures in Pool Boiling of Water." J. Heat Transfer. **83**: 245-254.
16. Moore, F. D., and Mesler, R. B. (1961). "The Measurement of Rapid Surface Temperature Fluctuation During Nucleate Boiling of Water." AIChE J. **7**: 620-624
17. Rogers, T. F., and Mesler, R. B. (1964). "An Experimental Study of Surface Cooling by Bubbles During Nucleate Boiling of Water." AIChE J. **10**: 656-660.
18. Sharp, R. R. (1964). "The Nature of Liquid Film Evaporation During Nucleate Boiling". NASA TN D-1997.
19. I. A. Raben, R. T. Beaubouef, and G. E. Commerford (1965). "A Study of Heat Transfer in Nucleate Pool Boiling of Water at Low Pressure." Chemical Engineering Progresses Symposium Series, 61(57), 249-257.
20. R.Cole, H.L.Shulman, (1966). "Bubble growth rates at high Jakob numbers." Int. J. Heat Mass Transfer 9, 1377-1390.
21. S.J.D. Van Stralen, R.Cole, W.M.Sluyter, M.S.Sohal (1975). "Bubble Growth Rates in Nucleate Boiling of Water at Subatmospheric Pressures." Int. J. Heat Mass Transfer 18, 655-669.
22. A.Niro, G.P.Beretta (1990). "Boiling Regimes in a Closed Two-Phase Thermosyphon." Int. J. Heat Mass Transfer 33(10), 2099-2110.
23. Wade R.McGillis, Van P.Carey, J.S.Fitch, W.R.Hamburgen (1991). "Pool Boiling on a Small Heat Dissipating Element in Water at Low Pressure." ASME/AIChE National Heat Transfer Conference, Minneapolis Minnesota.Enhancement Techniques for Water at Low Pressure. Seventh IEEE SEMI-THERM^{TM} Symposium.
24. Ng Kim Choon, Anutosh Chakraborty, Sai Maung Aye, Wang Xiaolin (2005). "New Pool boiling data for water at subatmospheric pressures: Experiments and correlation." Applied Thermal Engineering.
25. Wade R.McGillis, Van P.Carey(1991). "Enhancement Techniques for Water at Low Pressure." Seventh IEEE SEMI-THERM^{TM} Symposium.
26. J.Pakleza, M.C.Duluc , T.Kowalewski . "Experimental Investigation of vapor bubble growth."

27. T.Raad and J.E.Myers(1971). "Nucleation studies in pool boiling on thin plates using liquid crystals." A.I.Ch.E Jl 17, 1260-1261.
28. D.B.R.Kenning (1992). "Wall temperature patterns in nucleate boiling." Int. J. Heat Mass Transfer 35(1), 73-86.
29. W.Bergez (1995). "Nucleate Boiling on a thin heating plate: heat transfer and bubbling activity of nucleation site." Int. J. Heat Mass Transfer 38, 1788-1811.
30. D.B.R.Kenning, T.Kono, M.Wienecke (2001). "Investigation of boiling heat transfer by liquid crystal thermography." Experimental Thermal and Fluid Science 25,219-229.
31. D.B.R.Kenning , Youyou Yan (1996). "Pool boiling heat transfer on a thin plate: features revealed by liquid crystal thermography." Int. J. Heat Mass Transfer 39(15), 3117-3137.